ACTUATORS AND SENSORS IN STRUCTURAL DYNAMICS

W. GAWRONSKI
Jet Propulsion Laboratory
California Institute of Technology
Pasadena, CA 91109
U.S.A.

1. Introduction

Flexible structure dynamics depend on the location and gains of actuator and sensors. This fact is often underestimated, although it is an important factor in the planning of structural dynamic tests, and in designing structural controllers. In this work we describe the impact of actuators and sensors gains and locations on structural properties, which includes structural controllability and observability, and structural and modal norms. Using these properties we show how to detect a damage of structural members, how to place actuators and sensors for structural testing and control, and how to tune actuators or sensors to excite a selected mode or a set of selected modes. The reader can find background material in my book [5]. The analysis is conducted in modal state-space coordinates, which are described at the beginning of this paper.

2. Modal State-Space Representation

In this section both the standard and generalized state-space representations of a structure are discussed. Both representations are presented in modal coordinates.

2.1. STANDARD STATE-SPACE REPRESENTATION

Models of a linear time-invariant system are described in a standard form called state space representation, which is of the following form

$$\begin{aligned} \dot{x} &= Ax + Bu \\ y &= Cx \end{aligned} \tag{1}$$

In the above equations the N-dimensional vector x is called the state vector, the s-dimensional vector u is the system input, and the r-dimensional vector y is the system output. The A, B, and C matrices are real constant matrices of appropriate dimensions (A is $N \times N$, B is $N \times s$, and C is $r \times N$).

A structural model, however, is typically represented by the well-known second-order model. Let n_d be a number of degrees of freedom of the system, let r be a number of

outputs, and let s be a number of inputs. A flexible structure in nodal coordinates is represented by the following equation:

$$\begin{aligned} M\ddot{q} + D\dot{q} + Kq &= B_o u \\ y &= C_{oq} q + C_{ov}\dot{q} \end{aligned} \tag{2}$$

In this equation q is the $n_d \times 1$ displacement vector; u is the $s \times 1$ input vector, y is the output vector, $r \times 1$; M is the mass matrix, $n_d \times n_d$, D is the damping matrix, $n_d \times n_d$, and K is the stiffness matrix, $n_d \times n_d$. The input matrix B_o is $n_d \times s$, the displacement output matrix C_{oq} is $r \times n_d$, and the velocity output matrix C_{ov} is $r \times n_d$. The mass matrix is positive definite, and the stiffness and damping matrices are positive semidefinite. On details of the derivation of these types of equations see [14], and [7].

The same equation can be represented in modal coordinates. Define the matrix of mode shapes (or modal matrix) Φ of dimensions $n_d \times n$, which consists of n natural modes of a structure

$$\Phi = [\phi_1 \quad \phi_2 \quad \dots \quad \phi_n] \tag{3}$$

where ϕ_i, $i = 1,\dots,n$, is the ith modal vector. The modal matrix diagonalizes mass and stiffness matrices M and K, namely

$$M_m = \Phi^T M \Phi, \quad K_m = \Phi^T K \Phi \tag{4}$$

The matrices M_m and K_m are diagonal. The matrix M_m is called modal mass matrix, and K_m is modal stiffness matrix.

The same transformation can be applied to the damping matrix

$$D_m = \Phi^T D \Phi \tag{5}$$

where D_m is the modal damping matrix. This matrix is not always obtained diagonal. A damping matrix that can be diagonalized by the above transformation is called a matrix of proportional damping. For example, a linear combination of the stiffness and mass matrices, $D = \alpha_1 K + \alpha_2 M$, produces a proportional damping matrix, see [2], [7] (α_1 and α_2 are non-negative scalars).

The second-order structural model (2) can be also expressed in modal coordinates by introducing a new variable, q_m, called a modal displacement, such that

$$q = \Phi q_m \tag{6}$$

After some manipulations (see [5]) Eq.(2) is in the form

$$\begin{aligned} &\ddot{q}_m + 2Z\Omega\dot{q}_m + \Omega^2 q_m = B_m u \\ &y = C_{mq} q_m + C_{mv}\dot{q}_m \end{aligned} \tag{7}$$

In the above equation $\Omega = diag(\omega_1, \omega_2, \ldots, \omega_n)$ is the matrix of natural frequencies, Z is the modal damping matrix, $Z = diag(\zeta_1, \zeta_2, \ldots, \zeta_n)$, where ζ_i is the damping of the *i*th mode. The modal input matrix B_m is obtained as

$$B_m = M_m^{-1}\Phi^T B_c \tag{8}$$

and in Eq.(7) we used the following modal displacement and rate matrices

$$C_{mq} = C_{oq}\Phi, \quad C_{mv} = C_{ov}\Phi \tag{9}$$

Note that equation (7) is a set of uncoupled equations, since the matrices Ω and Z are diagonal. Thus, this set of equations can be re-written as follows

$$\begin{aligned} &\ddot{q}_{mi} + 2\zeta_i\omega_i\dot{q}_{mi} + \omega_i^2 q_{mi} = b_{mi} u \\ &y_i = c_{mqi} q_{mi} + c_{mvi}\dot{q}_{mi} \end{aligned} \tag{10}$$

$i = 1, \ldots, n$, where $y = \sum_{i=1}^{n} y_i$, b_{mi} is the *i*th row of B_m, and c_{mqi} , c_{mvi} are the *i*th columns of C_{mq} and C_{mv}, respectively. In the above equations y_i is the system output due to the *i*th mode dynamics. Note that the structural response y is a sum of modal responses y_i, which is a key property used to derive structural properties in modal coordinates.

Based on Eq.(10), the modal state-space representation (A_m, B_m, C_m) of a structure can be obtained, see [5]. It is characterized by the block-diagonal state matrix, A_m

$$A_m = \mathrm{diag}(A_{mi}) = \begin{bmatrix} \bullet & \bullet & 0 & 0 & \cdots & \cdots & 0 & 0 \\ \bullet & \bullet & 0 & 0 & \cdots & \cdots & 0 & 0 \\ 0 & 0 & \bullet & \bullet & \cdots & \cdots & 0 & 0 \\ 0 & 0 & \bullet & \bullet & \cdots & \cdots & 0 & 0 \\ \cdots & \cdots & \cdots & \cdots & \cdots & \cdots & \cdots & \cdots \\ \cdots & \cdots & \cdots & \cdots & \cdots & \cdots & \cdots & \cdots \\ 0 & 0 & 0 & 0 & \cdots & \cdots & \bullet & \bullet \\ 0 & 0 & 0 & 0 & \cdots & \cdots & \bullet & \bullet \end{bmatrix} \tag{11}$$

i = 1, 2, ..., n, where A_{mi} are 2×2 blocks (with non-zero elements marked by $\bullet$). The modal input and output matrices are divided accordingly

$$B_m = \begin{bmatrix} B_{m1} \\ B_{m2} \\ \vdots \\ B_{mn} \end{bmatrix}, \qquad C_m = \begin{bmatrix} C_{m1} & C_{m2} & \cdots & C_{mn} \end{bmatrix} \tag{12}$$

where B_{mi} and C_{mi} are $2 \times s$, and $r \times 2$ blocks, respectively.

The state x of the modal representation consists of n independent components, x_i, i.e., $x^T = \{x_1^T, \ x_2^T, \ \ldots \ x_n^T\}$. The ith component represents the ith mode, and consists of two states $x_i^T = \{x_{i1} \ \ x_{i2}\}$. The ith component, or mode, has its own state-space representation (A_{mi}, B_{mi}, C_{mi}), and is independently obtained from the following state equations

$$\begin{aligned} \dot{x}_i &= A_{mi} x_i + B_{mi} u \\ y_i &= C_{mi} x_i \end{aligned} \tag{13}$$

and $y = \sum_{i=1}^{n} y_i$.

Two modal representations can be distinguished. The first one, called modal model 1, has the component defined as follows

$$x_i = \begin{Bmatrix} \omega_i q_{mi} \\ \dot{q}_{mi} \end{Bmatrix}, \tag{14}$$

while the second one (modal model 2) as follows

$$x_i = \begin{Bmatrix} \omega_i q_{mi} \\ \zeta_i \omega_i q_{mi} + \dot{q}_{mi} \end{Bmatrix} \tag{15}$$

where q_{mi} and $\dot{q}_{mi}$ are the ith modal displacement and modal velocity.

The following state-space representation (A_{mi}, B_{mi}, C_{mi}) correspond to the above models

- modal model 1

$$A_{mi} = \begin{bmatrix} 0 & \omega_i \\ -\omega_i & -2\zeta_i \omega_i \end{bmatrix}, \qquad B_{mi} = \begin{bmatrix} 0 \\ b_{mi} \end{bmatrix}, \qquad C_{mi} = \begin{bmatrix} \dfrac{c_{mqi}}{\omega_i} & c_{mvi} \end{bmatrix} \tag{16}$$

- modal model 2

$$A_{mi} = \begin{bmatrix} -\zeta_i\omega_i & \omega_i \\ -\omega_i & -\zeta_i\omega_i \end{bmatrix}, \quad B_{mi} = \begin{bmatrix} 0 \\ b_{mi} \end{bmatrix}, \quad C_{mi} = \begin{bmatrix} \frac{c_{mqi}}{\omega_i} - c_{mvi}\zeta & c_{mvi} \end{bmatrix} \tag{17}$$

2.2. GENERALIZED STATE-SPACE REPRESENTATION

Here we consider a more complex model, which is used to describe a system under testing or control. It is called a generalized model, and consists of two *kinds* of inputs, denoted u and w, and of two *kinds* of outputs, denoted y and z, see Fig.1.

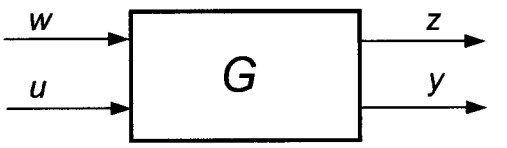

Figure 1. The generalized model consists of two inputs (u – actuator and w – disturbance) and two outputs (y – sensor, and z – performance)

The inputs to the generalized model consist of two vector signals:

- The actuator input, denoted u, which consists of all inputs handled by the controller, or applied as test inputs.
- The disturbance vector, w, which consists of noises and disturbances that are not part of the controller action or are not a part of the test input.

The outputs of the generalized model consist of two vector signals:

- The sensor vector, y: it is the controller feedback signal or the measured test signal.
- The performance vector, z: the signal that represents closed-loop performance or test performance.

The input and output selection in the generalized model are listed in Table 1.

TABLE 1. Inputs and outputs of a generalized model of a structure under testing or control

		Test	Control
Input	u	Test inputs (actuator signals)	Control inputs (produced by controller)
	w	Disturbances, all uncontrolled inputs	Disturbances and commands
Output	y	Measured variables (sensor signals)	Feedback signals accessed by controller
	z	Sensor noise, non-measurable performance outputs	Sensor noise, non-measurable performance outputs

Let A be the state matrix of the system, B_u and B_w are the input matrices of u and w, respectively, and C_y and C_z are the output matrices of y and z, respectively; then the state space representation of the generalized model is as follows

$$\begin{aligned} \dot{x} &= Ax + B_u u + B_w w \\ y &= C_y x, \\ z &= C_z z \end{aligned} \tag{18}$$

This model is transformed into the modal state-space representation the same way as the standard model previously described.

3. Controllability and Observability

System dynamics, excited at the input and measured at the output, are described by the state variables. However, the input may not be able to excite all states; consequently, it cannot fully control the system. Also, not all states may be represented at the output i.e., state dynamics may not be fully observed. Based on these two observations, we call a system controllable if the input excites all states and we call it observable if all the states are represented in the output

3.1. GRAMMIANS

We use grammians to evaluate the system controllability and observability properties. They are defined as follows (see, for example, [9], and [15])

$$W_c = \int_0^\infty e^{A\tau} BB^T e^{A^T\tau} d\tau, \quad W_o = \int_0^\infty e^{A^T\tau} C^T C e^{A\tau} d\tau \tag{19}$$

and are obtained from the Lyapunov equations:

$$AW_c + W_c A^T + BB^T = 0, \quad A^T W_o + W_o A + C^T C = 0 \tag{20}$$

For stable A, the obtained grammians W_c and W_o are positive definite.

The eigenvalues of the grammians change during the coordinate transformation. However, the eigenvalues of the grammian product are invariant. These invariants are denoted γ_i,

$$\gamma_i = \sqrt{\lambda_i(W_c W_o)}, \tag{21}$$

where $i = 1, \ldots, N$, and are called the Hankel singular values of the system.

3.2. BALANCED REPRESENTATION – WHERE ACTUATORS AND SENSORS ARE EQUALLY IMPORTANT

Consider a case when controllability and observability grammians are equal and diagonal (see [12]) i.e., when

$$W_c = W_o = \Gamma \tag{22}$$

where $\Gamma = \mathrm{diag}(\gamma_1, ..., \gamma_N)$, and $\gamma_i \geq 0$, i = 1, ..., N. The diagonal entries γ_i are called Hankel singular values of the system (earlier introduced as eigenvalues of product of the controllability and observability grammians). For a matrix that transforms a system into a balanced representation see [5].

The diagonality means that each state has an independent measure of controllability and observability. The equality means that each state is equally controllable and observable. The diagonality of grammians allows to evaluate each state (or mode) separately, and to determine how important they are for testing and for control purposes. Indeed, if a state is weakly controllable and, at the same time, weakly observable, it can be neglected without impacting the accuracy of analysis, dynamic testing, or control design procedures. On the other hand, if a state is strongly controllable and strongly observable, it must be retained in the system model in order to preserve accuracy of analysis, test, or control system design.

3.3. INPUT AND OUTPUT GAINS AS AN ALTERNATIVE MEASURE OF CONTROLLABILITY AND OBSERVABILITY

Consider the input and output matrices in modal coordinates, as in Eq.(12). Their two-norms, $\|B_m\|_2$ and $\|C_m\|_2$, are called the input and output gains of the structure

$$\|B_m\|_2 = \left(tr(B_m B_m^T)\right)^{\frac{1}{2}}, \quad \|C_m\|_2 = \left(tr(C_{mq}\Omega^{-2}C_{mq}^T + C_{mv}C_{mv}^T)\right)^{\frac{1}{2}} \tag{23}$$

They contain information on structural controllability and observability. Additionally, each mode has its own gain, namely $\|B_{mi}\|_2$, which is the input gain of the ith mode, and $\|C_{mi}\|_2$, which is the output gain of the ith mode, where B_{mi} and C_{mi} are given in modal coordinates, as in (16) and (17); thus, by definition

$$\|B_{mi}\|_2 = \left(tr(B_{mi}B_{mi}^T)\right)^{\frac{1}{2}} = \left(tr(b_{mi}b_{mi}^T)\right)^{\frac{1}{2}} \tag{24}$$

$$\|C_{mi}\|_2 = \left(tr(C_{mi}C_{mi}^T)\right)^{\frac{1}{2}} = \left(tr(\frac{c_{mqi}c_{mqi}^T}{\omega_i^2} + c_{mvi}c_{mvi}^T)\right)^{\frac{1}{2}} \tag{25}$$

It is easy to show that the gains of a structure are the root-mean-square sum of the modal gains

$$\|B_m\|_2 = \sqrt{\sum_{i=1}^{n} \|B_{mi}\|_2^2} \quad \text{and} \quad \|C_m\|_2 = \sqrt{\sum_{i=1}^{n} \|C_{mi}\|_2^2} \tag{26}$$

3.4. CONTROLLABILITY AND OBSERVABILITY OF A STRUCTURAL MODEL

In the following approximate relationships are used and denoted with the approximate equality sign "≅". They are applied in the following sense: two variables, x and y, are approximately equal ($x \cong y$) if $x = y + \varepsilon$ and $\|\varepsilon\| \ll \|y\|$.

Assuming small damping, the grammians in modal coordinates are diagonally dominant. This is expressed in the following property:

$$W_c \cong \mathrm{diag}(w_{ci} I_2), \quad W_o \cong \mathrm{diag}(w_{oi} I_2) \tag{27}$$

$i = 1,\ldots,n$, where $w_{ci} > 0$ and $w_{oi} > 0$ are the modal controllability and observability coefficients. Using this property the approximate Hankel singular values are obtained as a geometric mean of the modal controllability and observability coefficients

$$\gamma_i \cong \sqrt{w_{cii} w_{oii}} \tag{28}$$

The profiles of grammians and system matrix A in modal coordinates are drawn in Fig. 2.

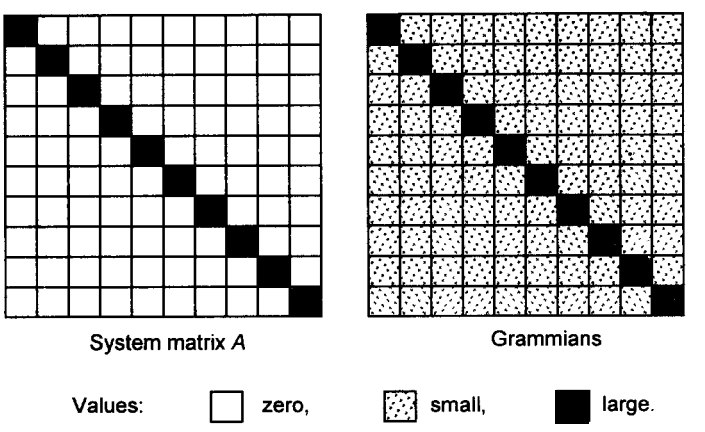

Figure 2. Profiles of the system matrix A (diagonal) and the grammians (diagonally dominant) in the modal coordinates.

Next, we express the grammians of each mode in a closed form. Let B_{mi} and C_{mi} be the $2\times s$ and $r\times 2$ blocks of B_m and C_m, then the diagonal entries of the controllability and observability grammians are as follows (for the derivation see [5]):

$$w_{ci} \cong \frac{\|B_{mi}\|_2^2}{4\zeta_i\omega_i}, \qquad w_{oi} \cong \frac{\|C_{mi}\|_2^2}{4\zeta_i\omega_i}, \tag{29}$$

Note from (29) that for a balanced structure the modal input and output gains are approximately equal

$$\|B_{mi}\| \cong \|C_{mi}\| \tag{30}$$

The approximate Hankel singular values are obtained from

$$\gamma_i \cong \frac{\|B_{mi}\|_2 \|C_{mi}\|_2}{4\zeta_i\omega_i} \tag{31}$$

Example 1. Comparing the exact and approximate Hankel singular values of the International Space Station structure. The input is a force at node marked by a white dot at the top of Fig. 3, and the output is a rate at this node. The results in Fig. 4 show good coincidence between the exact and approximate Hankel singular values.

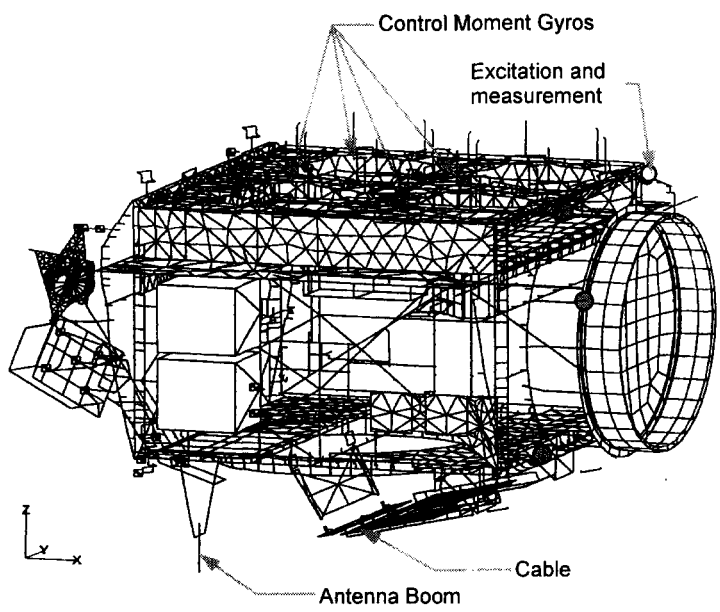

Figure 3. The finite element model of the International Space Station structure.

The closeness of the balanced and modal representations can be also observed in the closeness of the system matrix A in both representations. It was shown already that the matrix A in modal coordinates is diagonal (with 2×2 block on the diagonal). It can also be

shown, see [5], that the system matrix A in balanced coordinates is diagonally dominant with 2×2 blocks on the diagonal, while B, and C are divided into $2 \times s$ and $r \times 2$ blocks. The profiles of the grammians and a system matrix A are drawn in Fig. 5.

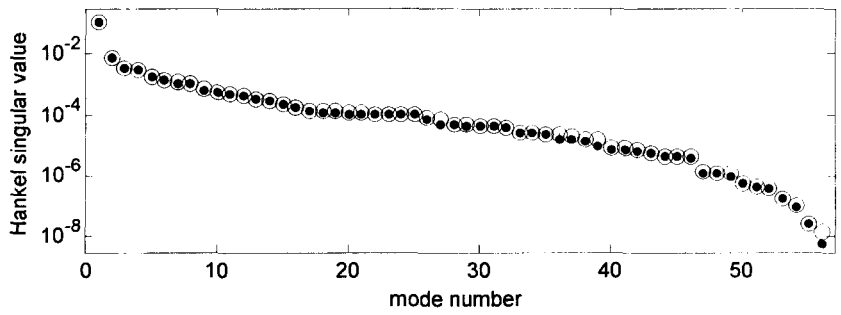

Figure 4. Exact (○) and approximate (•) Hankel singular values for the International Space Station structure are almost identical.

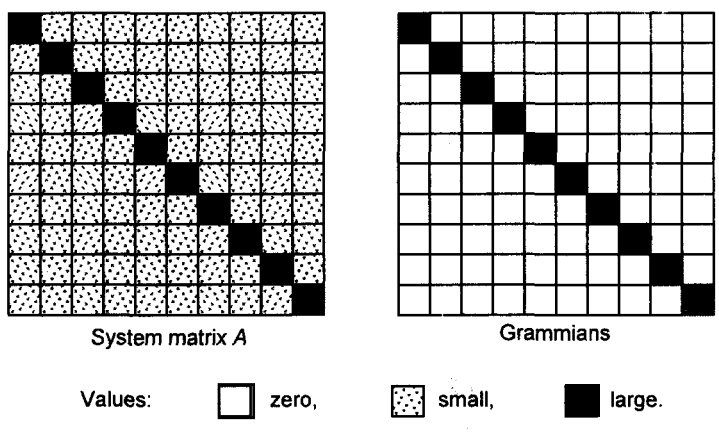

Figure 5. Profiles of the system matrix A (diagonally dominant) and the grammians (diagonal) in balanced coordinates.

4. Norms

System norms serve as measures of intensity of structural response to standard excitations, such as unit impulse, or white noise of unit standard deviation. The standardized response allows comparing different systems. We consider H_2, H_∞, and Hankel norms. It is shown that for flexible structures the H_2 norm has an additive property: it is a root-mean-square (rms) sum of the norms of individual modes. The H_∞ and Hankel norms are also determined from the corresponding modal norms, by selecting the largest one. On the other hand, all three norms of a mode with multiple inputs (or

outputs) can be decomposed into the rms sum of norms of a mode with a single input (or output). These two properties allow for the development of unique and efficient model reduction methods and actuator/sensor placement procedures.

4.1. DEFINITIONS OF SYSTEM NORMS

Let (A,B,C) be a state-space representation of a linear system and let $G(\omega) = C(j\omega I - A)^{-1}B$ be its transfer function. The H_2 norm of the system is defined as

$$\|G\|_2^2 = \frac{1}{2\pi}\int_{-\infty}^{\infty} \mathrm{tr}(G^*(\omega)G(\omega))d\omega \tag{32}$$

It can be interpreted as root-mean-square response of the system, performed over all the elements of the matrix transfer function and over all frequencies. A convenient way to determine the H_2 norm is to use the following formulas

$$\|G\|_2 = \sqrt{\mathrm{tr}(C^T C W_c)}, \quad \text{or,} \quad \|G\|_2 = \sqrt{\mathrm{tr}(BB^T W_o)} \tag{33}$$

where W_c and W_o are the controllability and observability grammians.

The H_∞ norm is defined as

$$\|G\|_\infty = \max_\omega \sigma_{\max}(G(\omega)) \tag{34}$$

where $\sigma_{\max}(G(\omega))$ is the largest singular value of $G(\omega)$. The H_∞ norm of a single-input–single-output system is the peak of the transfer function magnitude. It can be computed as a maximal value of ρ, such that the solution S of the following algebraic Riccati equation is positive definite, see [17], p.238

$$A^T S + SA + \rho^{-2} SBB^T S + C^T C = 0 \tag{35}$$

It is an iterative procedure where one starts with a large value of ρ and reduces it until negative eigenvalues of S appear.

The Hankel norm of a system is a measure of the effect of its past input on its future output [1, p. 103]. It is defined as

$$\|G\|_h = \sup_u \frac{\|y(t)\|_2}{\|u(t)\|_2}, \qquad \text{where} \qquad \begin{cases} u(t) = 0 & \text{for } t > 0 \\ y(t) = 0 & \text{for } t < 0 \end{cases} \tag{36}$$

It is determined from the controllability and observability grammians as follows

$$\|G\|_h = \sqrt{\lambda_{\max}(W_c W_o)} \tag{37}$$

where $\lambda_{\max}(.)$ denotes the largest eigenvalue. Thus, the Hankel norm of the system is therefore the largest Hankel singular value of the system, $\|G\|_h = \gamma_{\max}$.

4.2. NORMS OF A SINGLE MODE

For structures in the modal representation each mode is independent, thus the norms of a single mode are independent as well. Consider the *i*th natural mode and its state-space representation (A_{mi}, B_{mi}, C_{mi}), see(13). For this representation one obtains the following closed-form expression for the H_2 norm, see [5]:

$$\|G_i\|_2 \cong \frac{\|B_{mi}\|_2 \|C_{mi}\|_2}{2\sqrt{\zeta_i \omega_i}} \tag{38}$$

The H_∞ norm of a natural mode can be approximately expressed in the closed-form as follows:

$$\|G_i\|_\infty \cong \frac{\|B_{mi}\|_2 \|C_{mi}\|_2}{2\zeta_i \omega_i} \tag{39}$$

In order to prove this, note that the largest amplitude of the mode is approximately at the *i*th natural frequency, thus

$$\|G_i\|_\infty \cong \sigma_{\max}(G_i(\omega_i)) = \frac{\sigma_{\max}(C_{mi} B_{mi})}{2\zeta_i \omega_i} = \frac{\|B_{mi}\|_2 \|C_{mi}\|_2}{2\zeta_i \omega_i}$$

The Hankel norm is approximately obtained from the following formula:

$$\|G_i\|_h = \gamma_i \cong \frac{\|B_{mi}\|_2 \|C_{mi}\|_2}{4\zeta_i \omega_i} \tag{40}$$

Comparing the above equations one obtains the approximate relationships between H_2, H_∞, and Hankel norms of the *i*th mode

$$\|G_i\|_\infty \cong 2\|G_i\|_h \cong \sqrt{\zeta_i \omega_i}\, \|G_i\|_2 \tag{41}$$

The above relationship is illustrated in Fig.6.

Example 2. The determination of the H_2 norm for a simple system, as in Fig.7, is illustrated. For this system $m_1 = 11$, $m_2 = 5$, $m_3 = 10$, $k_1 = 10$, $k_2 = 50$, $k_3 = 55$, and $k_4 = 10$. The damping matrix is proportional to the stiffness matrix $D = 0.01K$. The single input u is applied to the three masses, such that $f_1 = u$, $f_2 = 2u$, $f_3 = -5u$, and the output is a linear combination of the mass displacements $y = 2q_1 - 2q_2 + 3q_3$, where q_i is the displacement of the *i*th mass and f_i is the force applied to that mass.

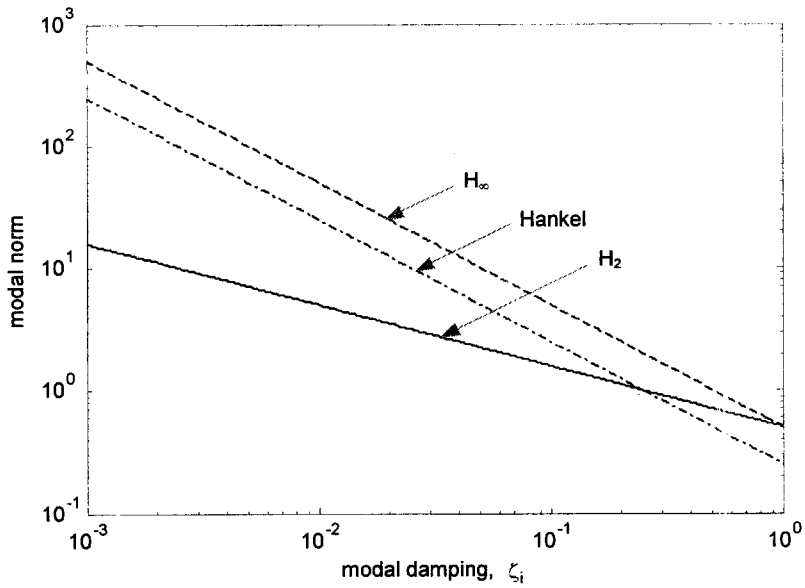

Figure 6. Modal norms versus modal damping

The transfer function of the system and of each mode is shown in Fig.8. It is observed that each mode is dominant in the neighborhood of the mode natural frequency, thus the system transfer function coincides with the mode transfer function near this frequency. The shaded area shown in Fig.9a is the H_2 norm of the second mode. Note that this area is shown in the logarithmic scale for visualization purposes and that most of the actual area is included in the neighborhood of the peak.

The H_2 norms of the modes determined from the (38) are: $\|G_1\|_2 = 1.9399$, $\|G_2\|_2 = 0.3152$, $\|G_3\|_2 = 0.4405$.

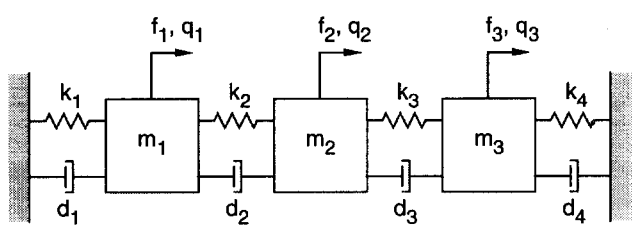

Figure 7. A simple structure.

Example 3. The determination of the H_∞ norm of a simple structure and its modes, as in Example 2, is illustrated. The H_∞ norm of the second mode is shown in Fig.9a as the height of the second resonance peak. The H_∞ norm of the system is shown in Fig.9b as the height of the highest (first in this case) resonance peak. The H_∞ norms of the modes, determined from (39) are: $\|G_1\|_\infty \cong 18.9229$, $\|G_2\|_\infty \cong 1.7454$, $\|G_3\|_\infty \cong 1.2176$.

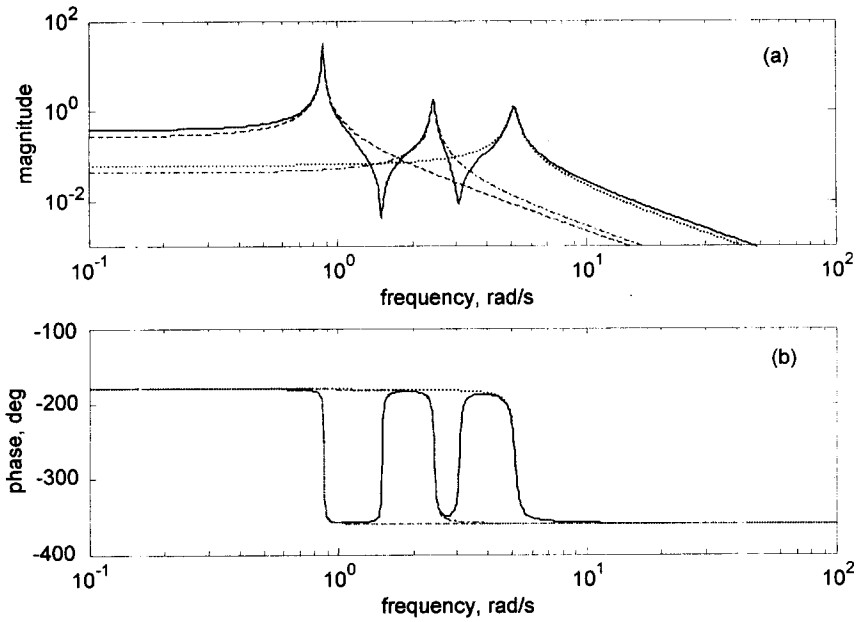

Figure 8. The transfer function of the system and of each mode.

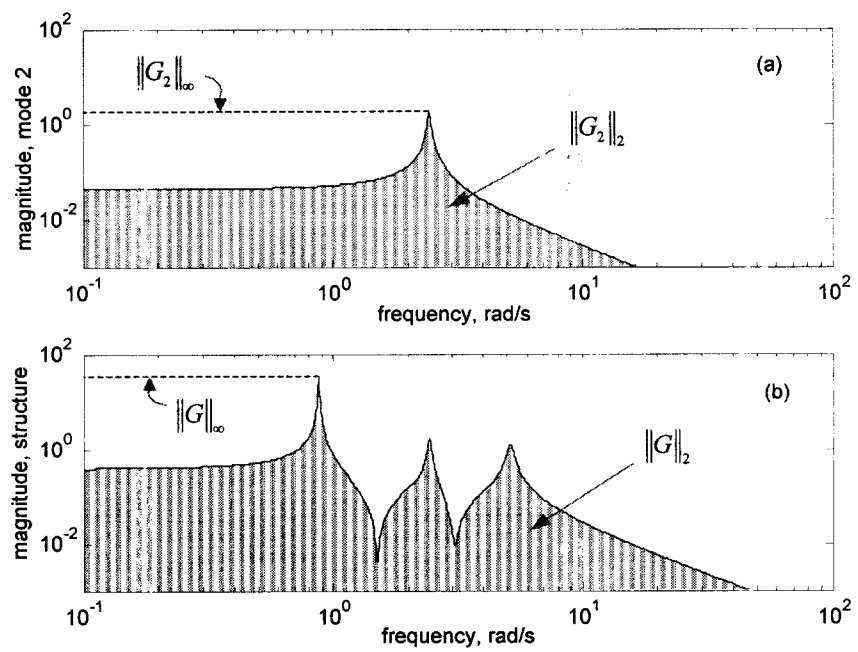

Figure 9. H_2 and H_∞ norms (a) of the second mode and (b) of the structure (single-input-single output case).

Example 4. Determination of the H_∞ norm of a single mode from the Ricccati equation (35). This norm is equal to the smallest positive parameter ρ for which the solution S of this equation is positive definite

Due to almost-independence of modes, the solution S of the Riccati equation is diagonally dominant, $S \cong diag(s_1, s_2, ..., s_n)$, where, by inspection, one can find s_i as a solution of the following equation

$$s_i(A_{mi} + A_{mi}^T) + s_i^2 \rho_i^{-2} B_{mi} B_{mi}^T + C_{mi}^T C_{mi} \cong 0,$$

where $i = 1, 2, ..., n$, and A_{mi} is given by Eq.(17), B_{mi} is two-row block of B_m corresponding to block A_{mi} of A_m, and C_{mi} is two-column block of C_m corresponding to block A_{mi} of A_m. For the balanced mode the Lyapunov equations (20) are

$$\gamma_i(A_{mi} + A_{mi}^T) + B_{mi} B_{mi}^T \cong 0, \qquad \gamma_i(A_{mi} + A_{mi}^T) + C_{mi}^T C_{mi} \cong 0$$

Introducing them to the previous equation we obtain

$$s_i(A_{mi} + A_{mi}^T) - s_i^2 \rho_i^{-2} \gamma_i (A_{mi} + A_{mi}^T) - \gamma_i (A_{mi} + A_{mi}^T) \cong 0$$

or, for a stable system

$$s_i^2 - \frac{\rho_i^2}{\gamma_i} s_i + \rho_i^2 \cong 0$$

with two solutions $s_i^{(1)}$ and $s_i^{(2)}$

$$s_i^{(1)} = \frac{\rho_i^2 (1 - \beta_i)}{2\gamma_i}, \quad s_i^{(2)} = \frac{\rho_i^2 (1 + \beta_i)}{2\gamma_i}, \quad \text{and} \quad \beta_i = \sqrt{1 - \frac{4\gamma_i^2}{\rho_i^2}}$$

For $\rho_i = 2\gamma_i$ one obtains $s_i^{(1)} = s_i^{(2)} = 2\gamma_i = \rho_i$. Moreover, $\rho_i = 2\gamma_i$ is the smallest ρ_i for which a positive solution s_i exists. It is indicated in Fig.10 by plots of $s_i^{(1)}$ (solid line) and $s_i^{(2)}$ (dashed line) versus ρ_i, and for $\gamma_i = 0.25$, 0.5, 1, 2, 3, and 4; the circle "O" denotes locations for which $\|G_i\|_\infty = \rho_{i\max} = 2\gamma_i$.

In order to obtain positive definite S, all s_i must be positive. Thus, the largest ρ_i from the set $\{\rho_1, \ \rho_2, \ \cdots \ \rho_n\}$ is the smallest one for which S is positive definite, which can be easily verified in Fig.10. Thus,

$$\|G\|_\infty = \max_i \rho_i \cong 2\gamma_{\max}.$$

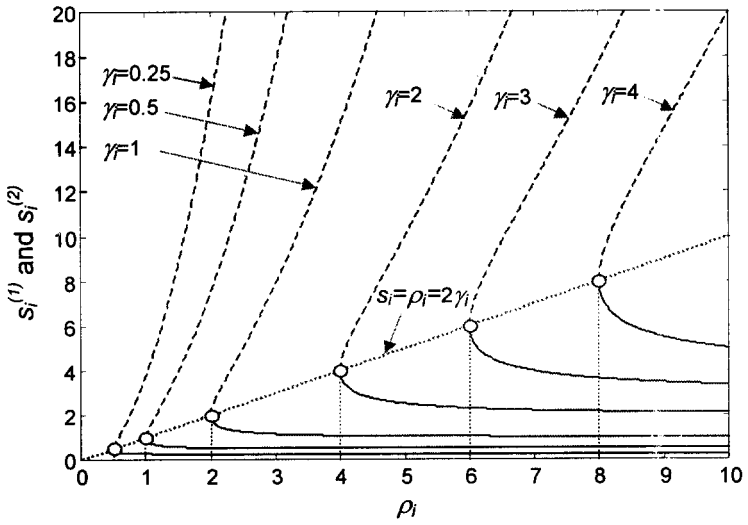

Figure 10. Solutions $s_i^{(1)}$ (solid lines) and $s_i^{(2)}$ (dashed lines); note that $\rho_i = 2\gamma_i$ at locations marked "O".

Example 5. H_∞, H_2 and Hankel norms of a truss. Consider a truss presented in Fig.11. Vertical control forces are applied at nodes 9 and 10, and the output rates are measured in the horizontal direction at nodes 4 and 5. For this structure, the H_2 and H_∞ norms of each mode are given in Fig.12a.

From (41) it follows that the ratio of the H_∞ and H_2 norms is

$$\frac{\|G_i\|_2}{\|G_i\|_\infty} \cong \sqrt{\zeta_i \omega_i} = 0.707\sqrt{\Delta\omega_i}$$

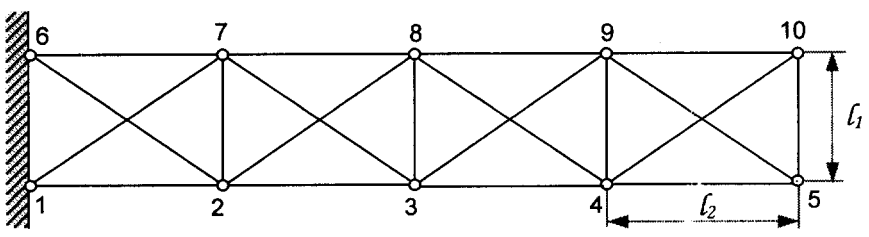

Figure 11. A 2D truss structure.

hence, the relationship between the H_∞ and H_2 norms depends on the width of the resonance. For a wide resonant peak the H_2 norm of the ith mode is larger than the corresponding H_∞ norm. For a narrow resonant peak the H_∞ norm of the ith mode is larger than the corresponding H_2 norm. This is visible in Fig.12a, where neither norm is dominant.

The exact Hankel singular values and the approximate values, obtained from (37) and (40), respectively, are shown in Fig. 12b. A good coincidence between the exact and approximate values is observed.

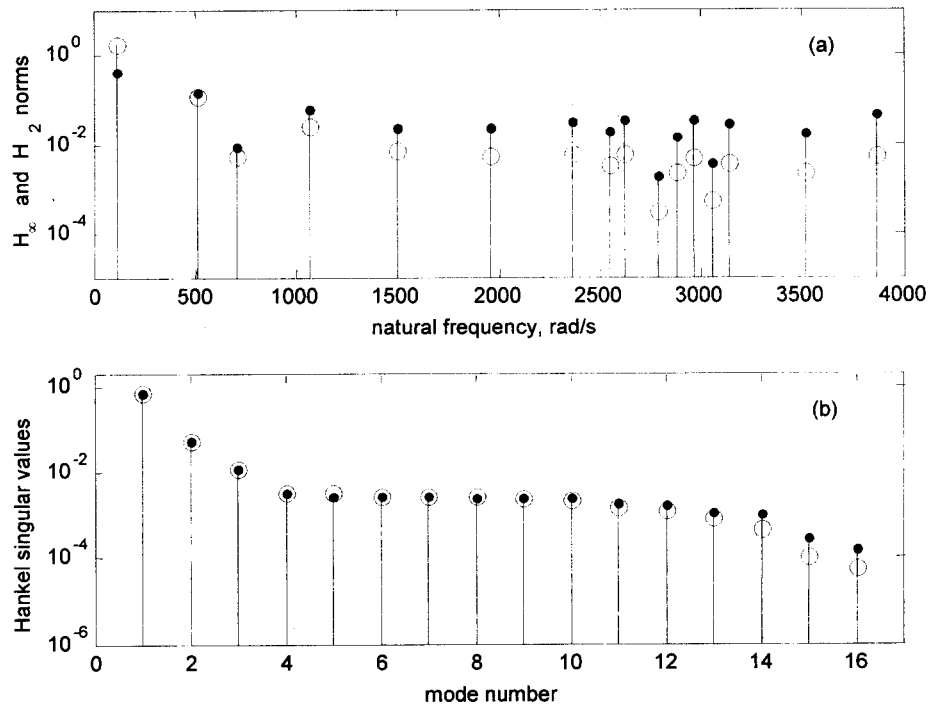

Figure 12. The 2D truss: (a) H_2 (○) and H_∞ (•) approximate norms, and (b) the exact (○) and the approximate (•) Hankel singular values.

4.3. NORMS OF A MODE WITH MULTIPLE ACTUATORS AND SENSORS

Above we considered norms of modes with multiple actuators and sensors. Here we continue to consider the same problem, but we decompose the norms into more elementary norms. Consider a flexible structure with s actuators and n modes, so that the modal input matrix B consists of n block-rows of dimension $2 \times s$

$$B_m = \begin{bmatrix} B_{m1} \\ B_{m2} \\ \vdots \\ B_{mn} \end{bmatrix} \tag{42}$$

and the ith block-row B_{mi} of B_m that corresponds to the ith mode has the form

$$B_{mi} = \begin{bmatrix} B_{mi1} & B_{mi2} & \cdots & B_{mis} \end{bmatrix} \tag{43}$$

where B_{mik} corresponds to the kth actuator at the ith mode.

Similarly to the actuator properties one can derive sensor properties. For r sensors of an n mode structure, the output matrix is as follows:

$$C_m = \begin{bmatrix} C_{m1} & C_{m2} & \ldots & C_{mn} \end{bmatrix}, \qquad C_{mi} = \begin{bmatrix} C_{m1i} \\ C_{m2i} \\ \vdots \\ C_{mri} \end{bmatrix} \tag{44}$$

where C_{mi} is the output matrix of the ith mode, and C_{mji} is the 1×2 block of the jth output at the ith mode.

Denote G_{mik} the ith mode with kth actuator only, i.e. with the state-space representation $(A_{mi}, B_{mik}, C_{mi})$. Let G_{mij} be a structure with jth sensor only, i.e. with the state-space representation $(A_{mi}, B_{mi}, C_{mij})$. The question arises as to how the norm of a mode with a single actuator or sensor corresponds to the norm of the same mode with multiple actuators or sensors.

We show that the H_2, H_∞, and Hankel norms of the ith mode with a set of s actuators is the rms sum of the corresponding norms of the ith mode with a single actuator, i.e.,

$$\|G_{mi}\| \cong \sqrt{\sum_{k=1}^{s} \|G_{mik}\|^2}, \qquad i = 1, \ldots, n. \tag{45}$$

where $\|.\|$ denotes either H_2, H_∞, or Hankel norm. In order to show it, note that the norm of the ith mode with the kth actuator and the norm of the ith mode with all actuators are

$$\|G_{mik}\| \cong \frac{\|B_{mik}\|_2 \|C_{mi}\|_2}{\alpha_i}, \qquad \|G_{mi}\| \cong \frac{\|B_{mi}\|_2 \|C_{mi}\|_2}{\alpha_i}$$

where $\alpha_i = 2\sqrt{\zeta_i \omega_i}$ for the H_2 norm, $\alpha_i = 2\zeta_i \omega_i$ for the H_∞ norm, and $\alpha_i = 4\zeta_i \omega_i$ for the Hankel norm. But, from the definition of the norm and from (43) it follows that

$$\|B_{mi}\|_2 = \sqrt{\sum_{k=1}^{s} \|B_{mik}\|_2^2}.$$

Introducing the above equation to the previous one, one obtains (45).

Similarly to the actuator properties one can derive sensor properties. For r sensors of n modes the output matrix is as in Eq.(44). For this output matrix the H_2, H_∞, and Hankel norms of the ith mode of a structure with a set of r sensors is the rms sum of the corresponding norms of the mode with each single actuator from this set, i.e.,

$$\|G_{mi}\| \cong \sqrt{\sum_{j=1}^{r} \|G_{mij}\|^2} \qquad (46)$$

$i = 1, \ldots, n$. These properties are illustrated in Fig.13a,b.

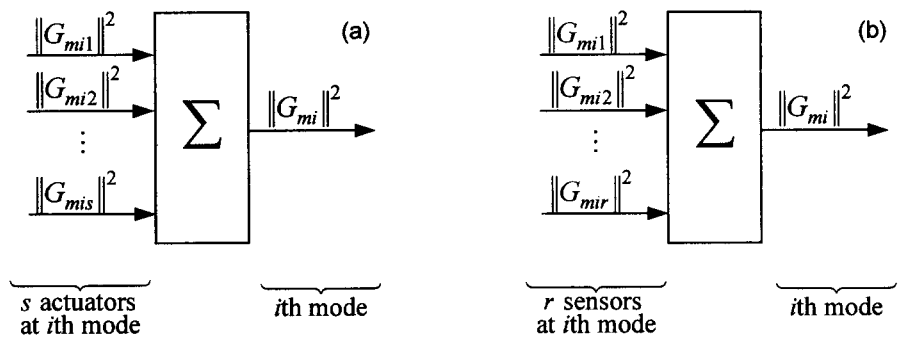

Figure 13. Decomposition of the H_2, H_∞, and Hankel norms of a mode into (a) actuator norms, and (b) sensor norms

4.4. NORMS OF AN ENTIRE STRUCTURE

The H_2, H_∞, and Hankel norms of the entire structure are expressed in terms of the norms of its modes. Let $G(\omega) = C_m(j\omega I - A_m)^{-1} B_m$ be the transfer function of a structure, and let (A_m, B_m, C_m) be its modal state-space representation. The system H_2 norm is, approximately, the rms sum of the modal norms

$$\|G\|_2 \cong \sqrt{\sum_{i=1}^{n} \|G_{mi}\|_2^2} \qquad (47)$$

where n is the number of modes.

In order to show it, note that the controllability grammian W_c in modal coordinates is diagonally dominant, thus the H_2 norm can be expanded as follows:

$$\|G\|_2^2 = \mathrm{tr}(C_m^T C_m W_c) \cong \sum_{i=1}^{n} \mathrm{tr}(C_{mi}^T C_{mi} W_{ci}) = \sum_{i=1}^{n} \|G_{mi}\|_2^2 .$$

Consider H_∞ norm of a structure in modal coordinates. Due to the independence of the modes, the system H_∞ norm is the largest of the mode norms, i.e.,

$$\|G\|_\infty \cong \max_i \|G_{mi}\|_\infty , \quad i = 1, \ldots, n. \qquad (48)$$

This property says that for a single-input-single-output system the largest modal peak response determines the worst-case response.

The Hankel norm of the structure is the largest norm of its modes, i.e.,

$$\|G\|_h \cong \max_i \|G_{mi}\|_h = \gamma_{\max} = 0.5\|G\|_\infty \tag{49}$$

where $\gamma_{\max}$ is the largest Hankel singular value of the system.

The above decompositions are illustrated in Fig.14 for actuators. A similar figure might be drawn for sensor norm decomposition.

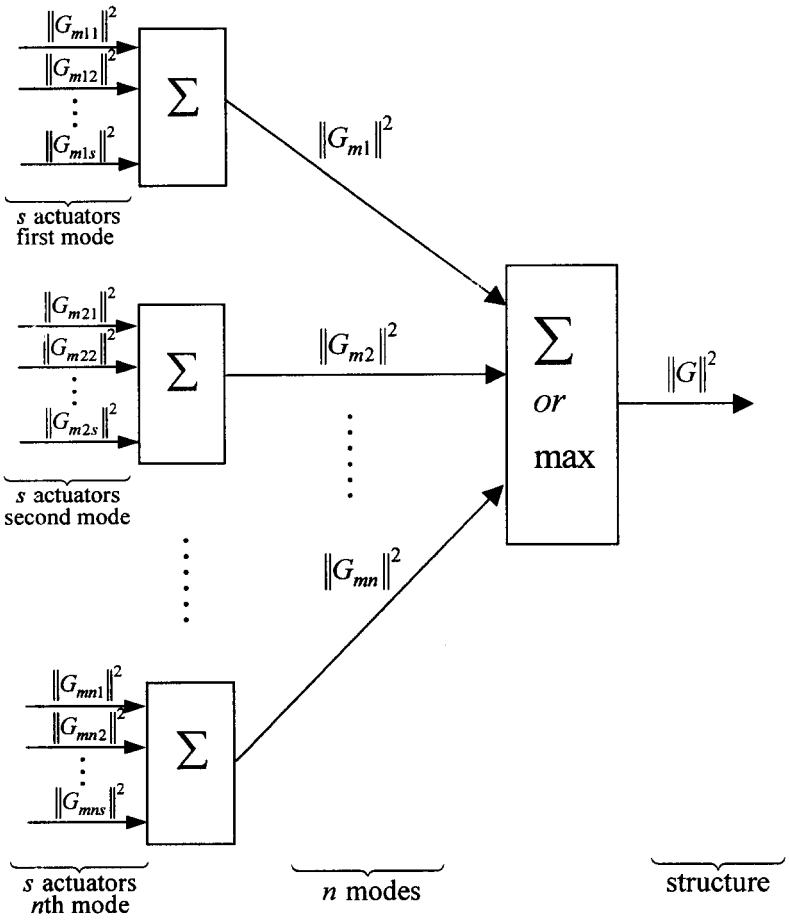

Figure 14. Combined decomposition of norms of a structure (H_2, H_∞, and Hankel) into modal norms and actuator norms

Example 6. Obtaining norms of the entire structure from modal norms. Using modal norms from Examples 2 and 3 find the H_2 and H_∞ norms of the structure.

The H_2 norm of the entire structure is represented by the shaded area in Fig.8b, which is approximately a sum of areas of each mode. We find from Eq.(47) that the approximate value of the system norm is the rms sum of modal norms, that is $\|G\|_2 \cong \sqrt{2.0141^2 + 0.3152^2 + 0.4405^2} = 2.0141$. This value is equal to the exact value of the system norm.

The H_∞ norm is the largest of the modal norms, see Eq.(48); using the results of Example 3 we found that the system norm is equal to the largest (first) modal norm, i.e., that $\|G\|_\infty = \|G_1\|_\infty \cong 18.9619$; it is equal to the exact value of the system norm computed independently.

Example 7. Using norms to detect structural damage. We illustrate the application of H_2 modal and sensor norms to determine damage locations. In particular, we localize damaged elements, and assess the modes particularly impacted by the damage.

Denote norm of the *j*th sensor of a healthy structure by $\|G_{shj}\|_2$, and norm of the *j*th sensor of a damaged structure by $\|G_{sdj}\|_2$. The *j*th sensor index of the structural damage is defined as a weighted difference between the *j*th sensor norms of a healthy and damaged structure, i.e.,

$$\sigma_{sj} = \frac{\left| \|G_{shj}\|_2^2 - \|G_{sdj}\|_2^2 \right|}{\|G_{shj}\|_2^2}$$

The sensor index reflects the impact of the structural damage on the *j*th sensor.

Similarly, denote the norm of the *i*th mode of a healthy structure by $\|G_{mhi}\|_2$, and the norm of the *i*th mode of a damaged structure by $\|G_{mdi}\|_2$. The *i*th mode index of the structural damage is defined as a weighted difference between the *i*th mode norm of a healthy and damaged structure, i.e.,

$$\sigma_{mi} = \frac{\left| \|G_{mhi}\|_2^2 - \|G_{mdi}\|_2^2 \right|}{\|G_{mhi}\|_2^2}$$

The *i*th mode index reflects impact of the structural damage on the *i*th mode.

A structure with fixed ends as in Fig.15 is analyzed. The cross section area of the steel beams is 1 cm^2. Two damage cases are considered. First, as a 20% reduction of the stiffness of the beam No 5, and the second case as a 20% reduction of the stiffness of the beam No17. The structure was more densely divided near the damage locations to better reflect the stress concentration. Nineteen strain-gage sensors are placed at the beams 1 to 19. A vertical force at node *P* excites the structure.

For the first case the sensor and the modal indices are shown in Fig.16a,b. The sensor indices in Fig.16a indicate that the sensor No 5, located at the damaged beam, suffered the most changes. The modal indices in Fig.16b show that the first mode was heavily affected by the damage.

The sensor and modal indices for the second case are shown in Fig.17a,b. Fig.17a shows the largest sensor index at location No 17, of the damaged beam. The modal indices in Fig.17b show that the tenth and the second modes were the most affected by the damage.

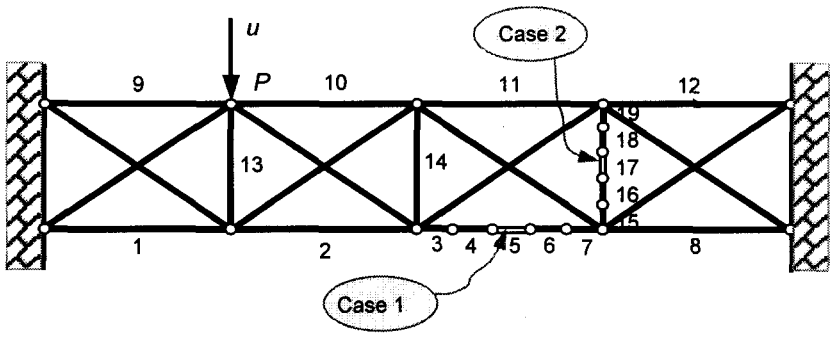

Figure 15. The beam structure: healthy elements are black, damaged elements are white, and numbers refer to the sensors.

4.5. NORMS OF A GENERALIZED STRUCTURE

Consider a structure as in Fig.1, with inputs w and u, and outputs z and y. Let G_{wz} be the transfer matrix from w to z, let G_{wy} be the transfer matrix from w to y, let G_{uz} be the transfer matrix from u to z, and let G_{uy} be the transfer matrix from u to y. Let G_{wzi}, G_{uyi}, G_{wyi}, and G_{uzi} be the transfer functions of the ith mode. The following multiplicative properties of modal norms hold:

$$\|G_{wzi}\|\|G_{uyi}\| \cong \|G_{wyi}\|\|G_{uzi}\| \tag{50}$$

In order to prove it, denote by B_{mw} and B_{mu} the modal input matrices of w and u, respectively; let C_{mz} and C_{my} be the modal output matrices of z and y, respectively; and let B_{mwi}, B_{mui}, C_{mzi}, and C_{myi} be their ith blocks related to the ith mode. The H_∞ norms are approximately determined from (39) as

$$\|G_{wzi}\| \cong \frac{\|B_{mwi}\|_2 \|C_{mzi}\|_2}{\alpha_i}, \qquad \|G_{uyi}\| \cong \frac{\|B_{mui}\|_2 \|C_{myi}\|_2}{\alpha_i},$$

$$\|G_{wyi}\| \cong \frac{\|B_{mwi}\|_2 \|C_{myi}\|_2}{\alpha_i}, \qquad \|G_{uzi}\| \cong \frac{\|B_{mui}\|_2 \|C_{mzi}\|_2}{\alpha_i}.$$

where $\alpha_i = 2\sqrt{\zeta_i \omega_i}$ for the H_2 norm, $\alpha_i = 2\zeta_i \omega_i$ for the H_∞ norm, and $\alpha_i = 4\zeta_i \omega_i$ for the Hankel norm. Introducing the above equations to (50), the approximate equality is proven by inspection.

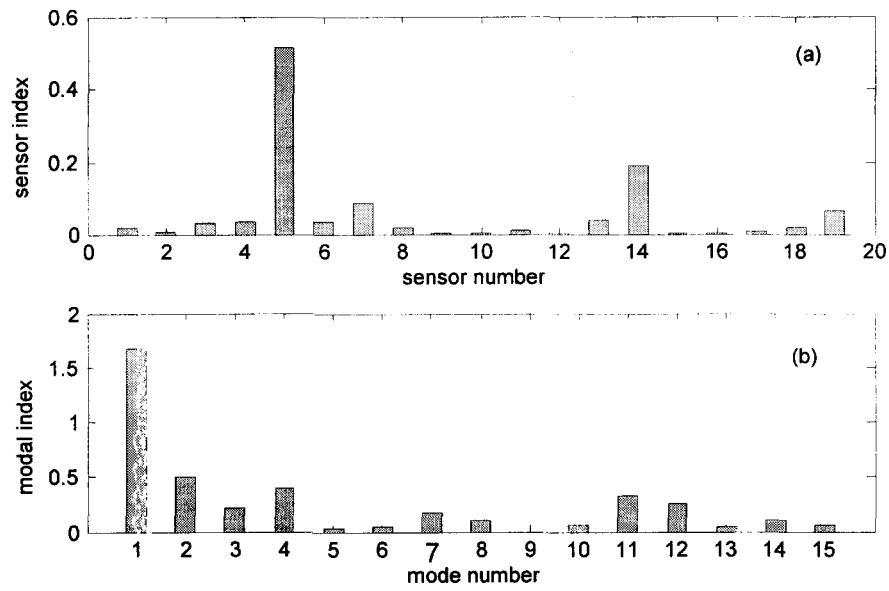

Figure 16. Sensor and modal indices for damage case 1: sensor index for the damaged element No 5 is high, modal index shows that the first mode is predominantly impacted.

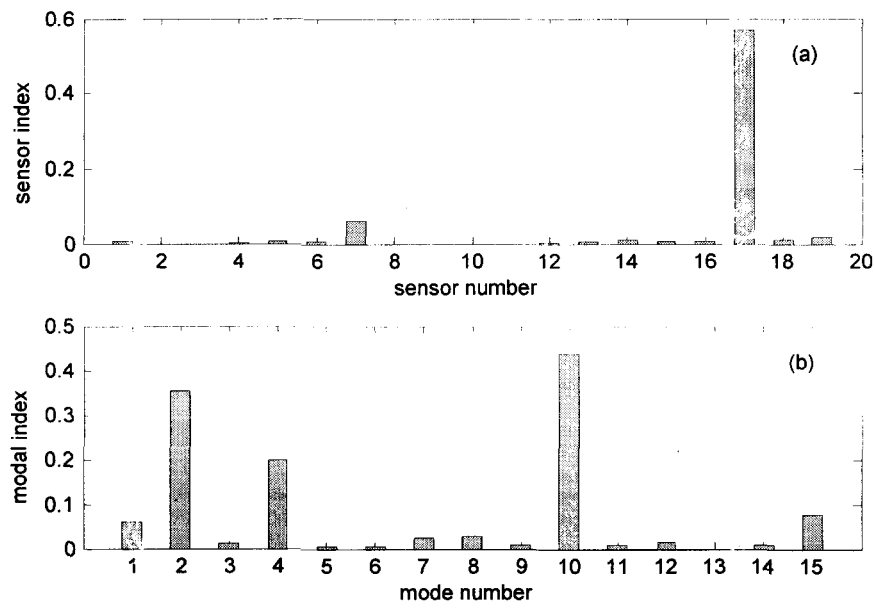

Figure 17. Sensor and modal indices for damage case 2: sensor index for the damaged element No 17 is high, modal index shows that the modes No 10, 2, and 4 are predominantly impacted.

The above property shows that for each mode the product of norms of the performance loop (i.e. from the disturbance to the performance) and the control loop (i.e. from the actuators to the sensors) is approximately equal to the product of the norms of the cross-couplings: between the disturbance and sensors, and between the actuators and performance. The physical meaning of this property lies in the fact that by increasing the actuator–sensor link, one increases automatically the cross-link: the actuator-performance link and the disturbance-sensors link. It shows that sensors not only respond to the actuator input but also to disturbances, and actuators not only impact the sensors but also the performance.

5. Model Reduction

Model reduction is a part of dynamic analysis, testing, and control. Typically, a model with a large number of degrees of freedom (developed for the static analysis) causes numerical difficulties in dynamic analysis, to say nothing of the high computational cost. In the system identification approach, on the other hand, the order of the identified system is determined by the reduction of the initially oversized model that includes a noise model. Finally, in structural control, the complexity and performance of a model-based controller depends on the order of the structural model. In all cases the reduction is a crucial part of the analysis and design. Thus, the reduced-order system solves the above problems if it acquires the essential properties of the full-order model.

In this section we consider structural model in modal coordinates, namely modal models 1 and 2, as in Eq.(16) and (17). The states of the model are as follows

$$x = \begin{Bmatrix} x_1 \\ x_2 \\ \vdots \\ x_n \end{Bmatrix} \tag{51}$$

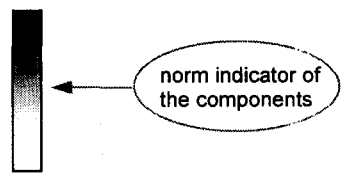

where x_i is the state corresponding to the ith mode. It consists of two states, see (14)

$$x_i = \begin{Bmatrix} x_{i1} \\ x_{i2} \end{Bmatrix} \tag{52}$$

Let $\|G_i\|$ denote either H_2, H_∞, or Hankel norm of the ith mode, and let the states in the state vector (51) be in the descending norm order. Now, the norm of the first mode is the largest one and the norm of the last mode is the smallest, which is marked in Eq.(51) with the norm value indicator (largest norm is indicated with black color, the smallest with white color).

A reduced-order model is obtained by evaluating the modal states and truncating the least important. Since the modes with the smallest norm are the last ones in the state vector, a reduced-order model is obtained here by truncating the last states in the modal

vector. How many of them? It depends on the system requirements, and is up to design engineer to check the reduced model accuracy. Let (A_m, B_m, C_m) be the modal representation corresponding to the modal state vector x as in (51). Let x be partitioned as follows:

$$x = \begin{Bmatrix} x_r \\ x_t \end{Bmatrix} \tag{53}$$

where x_r is the vector of the retained states, and x_t is a vector of truncated states. If there are $k < n$ retained modes, x_r is a vector of $2k$ states, and x_t is a vector of $2(n-k)$ states. Let the state triple (A_m, B_m, C_m) be partitioned accordingly,

$$A_m = \begin{bmatrix} A_{mr} & 0 \\ 0 & A_{mt} \end{bmatrix}, \qquad B_m = \begin{bmatrix} B_{mr} \\ B_{mt} \end{bmatrix}, \qquad C_m = \begin{bmatrix} C_{mr} & C_{mt} \end{bmatrix} \tag{54}$$

The reduced model is obtained by deleting the last $2(n-k)$ rows of A_m and B_m, and the last $2(n-k)$ columns of A_m and C_m.

Modal reduction by a truncation of a stable model always produces a stable reduced model, since the poles of the reduced model have not been changed.

Example 8. Reduction of the truss model. Consider a 2D truss as in Example 5. Its model is reduced in modal coordinates using the H_∞ norm. The approximate norms of the modes are shown in Fig. 18. From this figure the system norm (the largest of the mode norms) is $\|G\|_\infty = 1.6185$. Based on the modal norms it was decided that in the reduced-order model we reject all modes of the H_∞ norm less than 0.00003. The area where the H_∞ norm is less than 0.00003 lies below the dashed line in Fig.18, and the modes that have the H_∞ norm in this area are deleted. Consequently, the reduced model consists of three modes (No. 1,2, and 4). The transfer function of the full and reduced models (from the second input to the second output) is shown in Fig. 19a and the corresponding impulse response is shown in Fig. 19b. Both figures indicate a small reduction error, which is obtained as $(\|G\|_\infty - \|G_r\|_\infty)/\|G\|_\infty \cong \|G_4\|_\infty / \|G\|_\infty = 0.0040$.

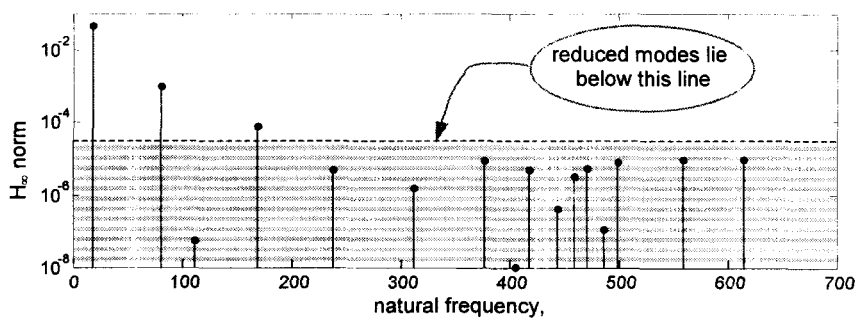

Figure 18. H_∞ norms of the 2D truss modes.

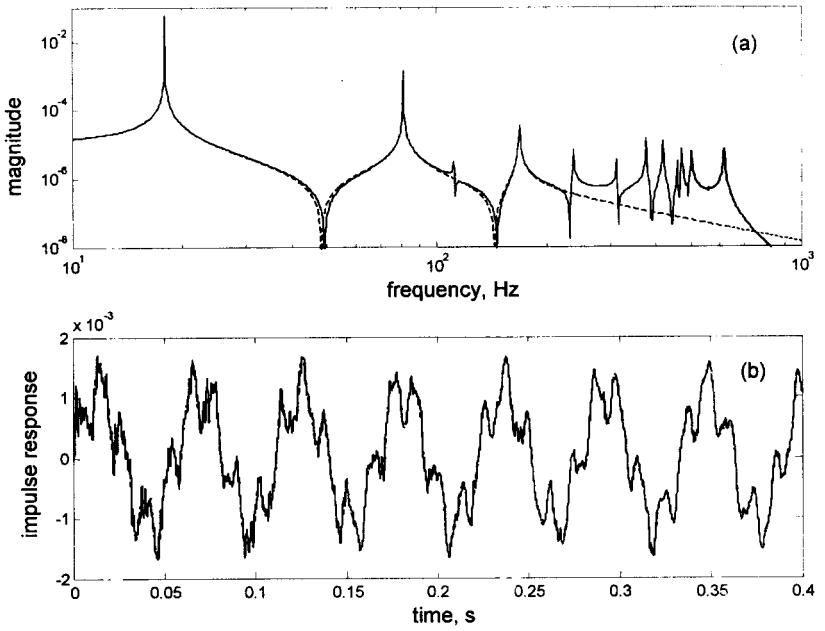

Figure 19. Magnitude of the transfer function (a), and impulse responses (b) of the full (solid line) and reduced (dashed line) truss models show that mainly the high-frequency modes were deleted, and overlapped impulse responses.

6. Actuator and Sensor Placement

A typical actuator and sensor location problem for structural testing can be described as a structural test plan. The plan is based on the available information on the structure itself, on disturbances acting on the structure, and on the expected structural performance. The preliminary information on structural properties is typically obtained from the finite-element model. The disturbance information includes disturbance location and disturbance spectral contents. The structure performance is commonly evaluated through the displacements or accelerations of selected structural locations.

In general it is not possible to duplicate the dynamics of a real structure during testing. This happens not only due to physical restrictions or limited knowledge of disturbances, but also because often the test actuators cannot be located at the location of actual disturbances and sensors cannot be placed at locations where the performance is evaluated. Thus, to conduct the test close to the real conditions, one uses the available (or candidate) locations of actuators and sensors and formulates the selection criteria and selection mechanisms.

The control design problem of a structure can be defined in a similar manner. Namely, actuators are placed at the allowable locations and they are not necessarily collocated with the locations where disturbances are applied; sensors are placed at the

sensor allowable locations, which are generally outside the locations where performance is evaluated.

For simple test articles, an experienced test engineer can determine the appropriate sensor or actuator locations in an ad hoc manner. However, for first-time testing of large and complex structures the placement of sensors and actuators is neither an obvious nor a simple task. In practice, heuristic means are combined with engineering judgment and simplified analysis to determine actuator and sensor locations. In most cases the locations vary during tests (in a trial and error approach) to obtain acceptable data to identify target modes. The actuator and sensor placement problem was investigated by many researchers, as reported in a review article [16].

For a small number of sensors or actuators a typical solution to the location problem is found through a search procedure. For large numbers of locations the search for the number of possible combinations is overwhelming, time consuming and does not necessarily give the optimal solution. The approach proposed here consists of the determination of the norm of each sensor (or actuator) for selected modes and then grade them according to their participation in the system norm. This is a computationally fast (non-search) procedure with a clear physical interpretation.

6.1. PROBLEM STATEMENT

Given a larger set of sensors and actuators, the placement problem consists of determining the locations of a smaller subset of sensors or actuators such that the H_2, H_∞, or Hankel norms of the subset are as close as possible to the norm of the original set. In this chapter this placement problem is solved in the modal coordinates.

Let $\mathcal{R}$ and S be the sets of the candidate sensor and actuator locations, chosen in advance as allowable locations of actuators of population S and as allowable locations of sensors of population R. The placement of s actuators from S actuator candidate locations, and the placement of r sensors from R sensor candidate locations is considered. Of course, the number of candidate locations is larger than the number of final locations, i.e., $R > r$ and $S > s$.

6.2. PLACEMENT INDICES AND MATRICES

Actuator and sensor placement problems are solved independently, however both procedures are similar. Denote the H_2, H_∞, or Hankel norms of the ith mode with the jth actuator only or the ith mode with the kth sensor only

$$\|G_{ij}\| = \frac{\|B_{mij}\|_2 \|C_{mi}\|_2}{\alpha_i}, \qquad \|G_{ik}\| = \frac{\|B_{mi}\|_2 \|C_{mki}\|_2}{\alpha_i} \tag{55}$$

where $\alpha_i = 2\sqrt{\zeta_i \omega_i}$ for the H_2 norm, $\alpha_i = 2\zeta_i \omega_i$ for the H_∞ norm, and $\alpha_i = 4\zeta_i \omega_i$ for the Hankel norm. Denoted by G is the transfer function of the system with all S candidate actuators. The placement index σ_{ki} that evaluates the kth actuator at the ith mode in terms of either H_2, H_∞, or Hankel norm is defined with respect to all the modes and all admissible actuators

$$\sigma_{ki} = w_{ki} \frac{\|G_{ki}\|}{\|G\|} \tag{56}$$

where $\|.\|$ denotes H_2 , H_∞, or Hankel norm, respectively, and $k = 1, ..., S$, $i = 1, ..., n$, and where $w_{ki} \geq 0$ is the weight assigned to the kth actuator and the ith mode n is a number of modes and G_{ki} is the transfer function of the ith mode and of the kth actuator. The weight reflects the importance of the mode and the actuator in applications. We evaluate actuator importance using a placement matrix in the following form

$$\Sigma = \begin{array}{c} \begin{bmatrix} \sigma_{11} & \sigma_{12} & \cdots & \sigma_{1k} & \cdots & \sigma_{1S} \\ \sigma_{21} & \sigma_{22} & \cdots & \sigma_{2k} & \cdots & \sigma_{2S} \\ \cdots & \cdots & \cdots & \cdots & \cdots & \cdots \\ \sigma_{i1} & \sigma_{i2} & \cdots & \sigma_{ik} & \cdots & \sigma_{iS} \\ \cdots & \cdots & \cdots & \cdots & \cdots & \cdots \\ \sigma_{n1} & \sigma_{n2} & \cdots & \sigma_{nk} & \cdots & \sigma_{nS} \end{bmatrix} \begin{array}{l} \\ \\ \\ \leftarrow i\text{th mode} \\ \\ \\ \end{array} \\ \uparrow \\ k\text{th actuator} \end{array} \tag{57}$$

The kth column of the above matrix consists of indexes of the kth actuator for every mode and the ith row is a set of the indexes of the ith mode for all actuators.

Similarly to actuators, the sensor placement index σ_{ki} evaluates the kth sensor at the ith mode

$$\sigma_{ki} = w_{ki} \frac{\|G_{ki}\|}{\|G\|} \tag{58}$$

$k = 1, ..., R$, $i = 1, ..., n$, where $w_{ki} \geq 0$ is the weight assigned to the kth sensor and the ith mode, n is a number of modes, and G_{ki} is the transfer function of the ith mode and kth sensor. The sensor placement matrix is defined as follows

$$\Sigma = \begin{array}{c} \begin{bmatrix} \sigma_{11} & \sigma_{12} & \cdots & \sigma_{1k} & \cdots & \sigma_{1R} \\ \sigma_{21} & \sigma_{22} & \cdots & \sigma_{2k} & \cdots & \sigma_{2R} \\ \cdots & \cdots & \cdots & \cdots & \cdots & \cdots \\ \sigma_{i1} & \sigma_{i2} & \cdots & \sigma_{ik} & \cdots & \sigma_{iR} \\ \cdots & \cdots & \cdots & \cdots & \cdots & \cdots \\ \sigma_{n1} & \sigma_{n2} & \cdots & \sigma_{nk} & \cdots & \sigma_{nR} \end{bmatrix} \begin{array}{l} \\ \\ \\ \leftarrow i\text{th mode} \\ \\ \\ \end{array} \\ \uparrow \\ k\text{th sensor} \end{array} \tag{59}$$

where the kth column consists of indexes of the kth sensor for every mode and the ith row is a set of the indexes of the ith mode for all sensors.

The placement matrix gives an insight into the placement properties of each actuator since the placement index of the kth actuator is determined as the rms sum of the kth column of Σ. The vector of the actuator placement indices is defined as $\sigma_a = [\sigma_{a1} \quad \sigma_{a2} \quad \dots \quad \sigma_{aS}]^T$ and its kth entry is the placement index of the kth actuator. In the case of the H_2 norm, it is the rms sum of the kth actuator indexes over all modes

$$\sigma_{ak} = \sqrt{\sum_{i=1}^{n} \sigma_{ik}^2}, \qquad k = 1, \dots, S \tag{60}$$

In the case of the H_∞ and Hankel norms, it is the largest index over all modes

$$\sigma_{ak} = \max_i(\sigma_{ik}), \qquad i = 1, \dots, n, \quad k = 1, \dots, S \tag{61}$$

Similarly, the vector of the sensor placement indices is defined as $\sigma_s = [\sigma_{s1} \quad \sigma_{s2} \quad \dots \quad \sigma_{sR}]^T$ and its kth entry is the placement index of the kth sensor. In the case of the H_2 norm, it is the rms sum of the kth sensor indexes over all modes

$$\sigma_{sk} = \sqrt{\sum_{i=1}^{n} \sigma_{ik}^2}, \qquad k = 1, \dots, R \tag{62}$$

In the case of the H_∞ and Hankel norms, it is the largest index over all modes

$$\sigma_{sk} = \max_i(\sigma_{ik}), \qquad i = 1, \dots, n, \quad k = 1, \dots, R \tag{63}$$

The vector of the mode indices is defined as follows: $\sigma_m = [\sigma_{m1} \quad \sigma_{m2} \quad \dots \quad \sigma_{mn}]^T$, and its ith entry is the index of the ith mode. This entry is an rms sum of the ith mode indices over all actuators

$$\sigma_{mi} = \sqrt{\sum_{k=1}^{S} \sigma_{ik}^2}, \qquad i = 1, \dots, n \tag{64}$$

or an rms sum of the ith mode indices over all sensors

$$\sigma_{mi} = \sqrt{\sum_{k=1}^{R} \sigma_{ik}^2}, \qquad i = 1, \dots, n \tag{65}$$

- The actuator placement index, σ_{ak}, is a nonnegative contribution of the kth actuator at all modes to the H_2, H_∞, or Hankel norms of the structure.

- The sensor placement index, σ_{sk}, is a nonnegative contribution of the *k*th sensor at all modes to the H_2, H_∞, or Hankel norms of the structure.
- The mode index, σ_{mi}, is a nonnegative contribution of the *i*th mode for all actuators (or all sensors) to the H_2, H_∞, or Hankel norms of the structure.

The determination of the H_∞ actuator and modal indices for the pinned beam is illustrated in Fig.20. Six actuators are located on the beam and four modes are considered. The second mode index is the rms sum of indices of all actuators for this mode and the third actuator index is the largest of these actuator indices over four modes. From the above properties it follows that the index σ_{ak} (σ_{sk}) characterizes the importance of the *k*th actuator (sensor), thus it serves as the actuator (sensor) placement index. Namely, the actuators (sensors) with small index σ_{ak} (σ_{sk}) can be removed as the least significant ones. Note also that the mode index σ_{mi} can also be used as a reduction index. Indeed, it characterizes the significance of the *i*th mode for the given locations of sensors and actuators. The norms of the least significant modes (those with the small index σ_{mi}) should either be enhanced by the reconfiguration of the actuators or sensors, or be eliminated.

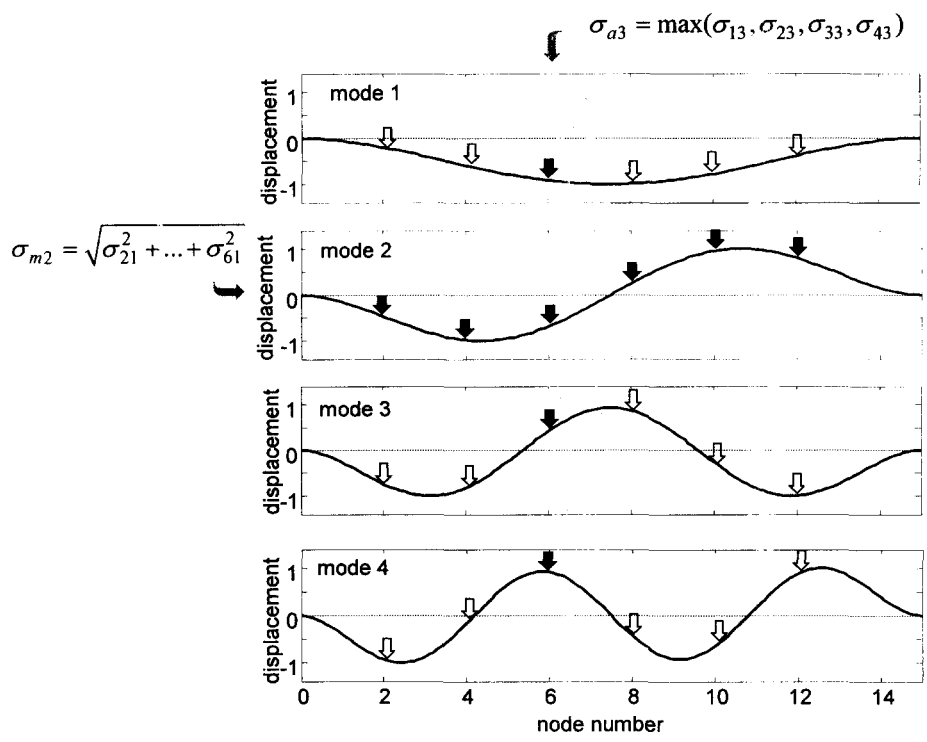

Figure 20. The determination of the H_∞ actuator and modal indices of a pinned beam (⇩ – actuator location; and ⬇ – actuators used for the calculation of the indices); the second mode index is the rms sum of indices of all six actuators for this mode, while the third actuator index is the largest of this actuator indices over all four modes.

Example 9. Placing sensors on a beam to detect up to four modes. Consider a beam as shown in Fig.21 with a vertical force at node 6. By using the placement technique presented above and the H_∞ norm, one shall find the best places for displacement sensors in the y-direction to sense the first, second, third, and fourth mode; and to sense simultaneously the first two modes, the first three modes, and the first four modes.

Each node of a beam has 3 degrees of freedom: horizontal displacement x, vertical displacement y, and rotation in the figure plane θ. Denote a unit vector $e_i = [0,0,\ldots,1,\ldots,0]$ that has all zeros except 1 at the ith location, then the displacement output matrix for sensors located at ith node is $C_{qij}^T = e_{3i-1}$. The input matrix is $B_o = e_{17}^T$.

The H_∞ norm $\|G_{ki}\|_\infty$ for the kth mode (k=1,2,3,4) and ith sensor location is obtained from (55) using B_o and C_{qi} as above. From these norms the sensor placement indices for each mode are obtained from (58), using weight such that $\max_i(\sigma_{\infty ki}) = 1$.

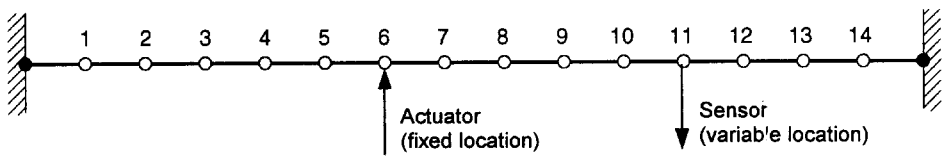

Figure21. A beam with a fixed actuator and a moving sensor.

The plots of $\sigma_{\infty ki}$ are shown in Fig.22a,b,c,d. The plot of the sensor indices for the first mode is shown in Fig.22a. It shows the maximum at node 7 or 8, indicating that the sensors shall be placed at these nodes. The plot of the sensor placement indices for the second mode is shown in Fig.22b. It shows two maximal values, at nodes 4 and 11, indicating these two locations as the best for sensing the second mode. The plot of the sensor placement indices for the third mode is shown in Fig.22c, showing two maximal values at nodes 3 and 7, indicating that these two locations are the best for sensing the third mode. Finally, the plot of the sensor placement indices for the fourth mode is shown in Fig.22d. It shows 4 maximal values at nodes 2, 6, 9, and 13, indicating that these four locations are the best for sensing the fourth mode.

Next, the indices for the first two modes are determined using Eq.(61), namely $\sigma_{\infty 12i} = \max(\sigma_{\infty 1i}, \sigma_{\infty 2i})$. The plot of this index is shown in Fig.23b with the index reaching its maximum at four locations: 4, 7, 8, and 11. These locations are the best for sensing the first and the second modes. Clearly, locations 7 and 8 serve for first mode sensing, while locations 4 and 11 serve for second mode sensing.

Next, the indices for the first three modes are determined, using Eq.(61), i.e., $\sigma_{\infty 123i} = \max(\sigma_{\infty 1i}, \sigma_{\infty 2i}, \sigma_{\infty 3i})$. The plot of this index is shown in Fig.23c with the index reaching its maximum at six locations: 3, 4, 7, 8, 11 and 12. These locations are the best for sensing the first, second, and third modes. Obviously, locations 7 and 8 serve for first mode sensing, locations 4 and 11 serve for second mode sensing, and locations 3 and 12 serve for third mode sensing.

Finally, the indices for the first four modes are determined using Eq.(61), $\sigma_{\infty 1234i} = \max(\sigma_{\infty 1i}, \sigma_{\infty 2i}, \sigma_{\infty 3i}, \sigma_{\infty 4i})$. The plot of this index is shown in Fig.23d, with the index reaching its maximum at eight locations: 2, 3, 4, 7, 8, 11, 12, and 13. These locations are the best for sensing the first, second, third, and fourth modes. Locations 7 and 8 serve for first mode sensing, locations 4 and 11 serve for second mode sensing, locations 3 and 12 serve for third mode sensing, and locations 2 and 13 serve for fourth mode sensing.

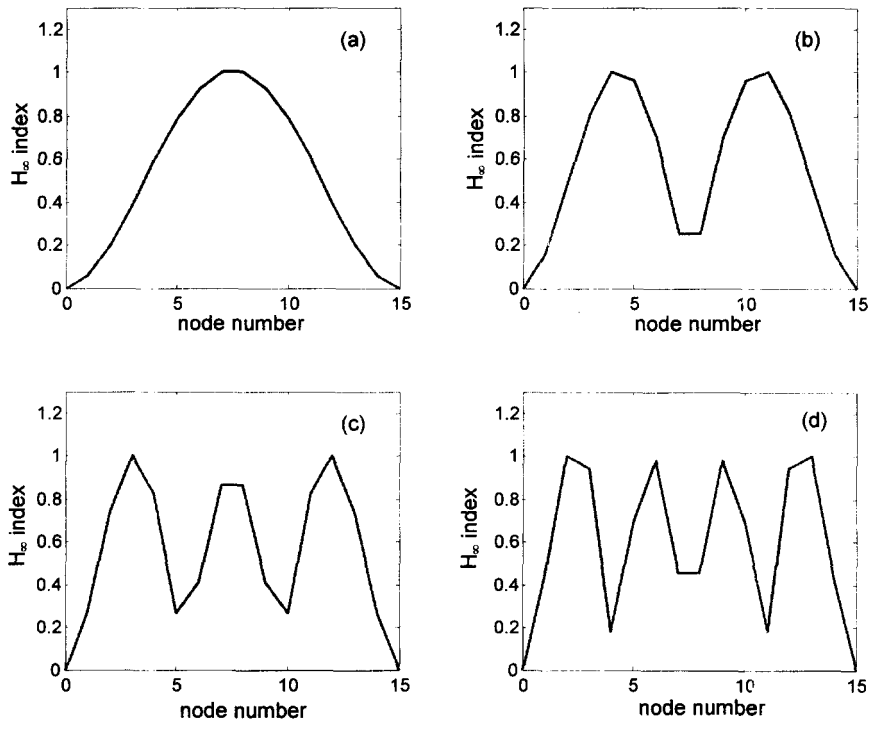

Figure22. H_∞ indices as a function of sensor locations: (a) for the first beam mode, (b) for the second beam mode, (c) for the third beam mode, and (d) for the fourth beam mode.

So far in this example we used the H_∞ norms and indices. It is interesting to compare the sensor placement using the H_2 norms and indices. First, the H_2 norm $\|G_{ki}\|_2$ for the kth mode (k=1,2,3,4) and ith sensor location is obtained from(55) using B_o and C_{qi} as above. Next, the indices for the first two modes are determined using Eq.(62), namely $\sigma_{2,12i} = \sqrt{\sigma_{2,1i}^2 + \sigma_{2,2i}^2}$. The plot of this index is shown in Fig.24b, where the index reaches its maximum at locations 5 and 10. Next, the indices for the first three modes are determined, using Eq.(62), i.e. $\sigma_{2,123i} = \sqrt{\sigma_{2,1i}^2 + \sigma_{2,2i}^2 + \sigma_{2,3i}^2}$. The plot of this index is shown in Fig.24c, where the index reaches its maximum at locations 4 and 11. Finally, the indices for the first four modes are determined using Eq.(62), i.e.

$\sigma_{2,1234i} = \sqrt{\sigma_{2,1i}^2 + \sigma_{2,2i}^2 + \sigma_{2,3i}^2 + \sigma_{2,4i}^2}$. The plot of this index is shown in Fig.24d, where the index reaches its maximum at locations 3 and 12.

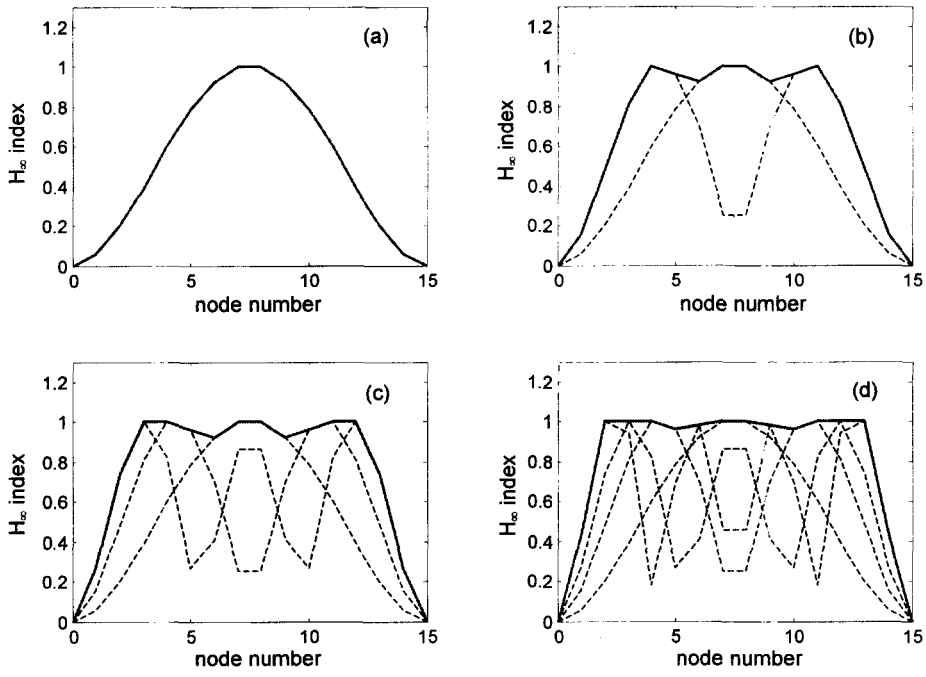

Figure 23. H_∞ sensor placement indices as a function of sensor locations: (a) for the first mode, (b) for the first two modes, (c) for the first three modes, and (d) for the first four modes.

A comparison of the H_∞ and H_2 indices in Fig.23 and Fig.24 shows that the H_2 index variation is more dramatic with the change of sensor location, while the H_∞ index variations are flatter (as the result of selection of maximal values). Thus the first index is a more sensitive measure of the sensor (or actuator) location. Due to the flattening action of the H_∞ norm, the H_∞ indices show slightly different sensor locations.

6.3. PLACEMENT FOR A GENERALIZED STRUCTURE

The problem of actuator and sensor placement presented in this section refers to the generalized structure. For this model we derive the placement rules based on the properties of the structural norms and illustrate their application with the truss sensor location. Consider a structure as in Fig.1 with inputs w and u, and outputs z and y. Denote G_{wz} as the transfer matrix from w to z, G_{wy} as the transfer matrix from w to y, G_{uz} as the transfer matrix from u to z, and G_{uy} as the transfer matrix from u to y. Denote G_{wzi}, G_{uyi}, G_{wyi}, and G_{uzi} as the transfer functions of the ith mode.

The following multiplicative properties of modal norms hold:

$$\|G_{wzi}\|\|G_{uyi}\| \cong \|G_{wyi}\|\|G_{uzi}\| \tag{66}$$

for $i = 1, \ldots, n$, where $\|.\|$ denotes either H_2, H_∞, or Hankel norms.

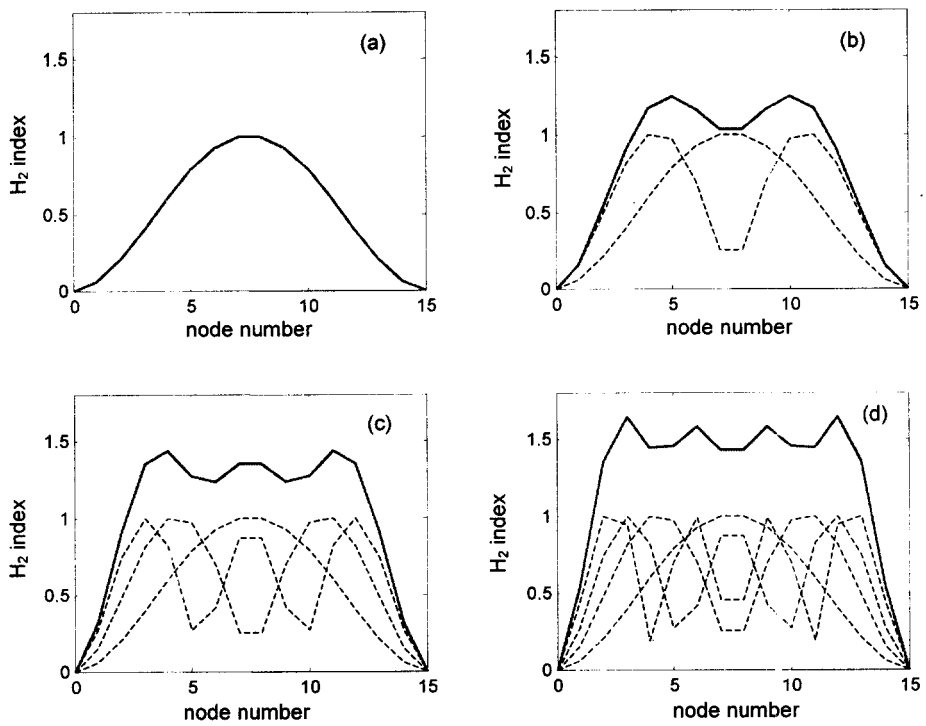

Figure 24. H_2 sensor placement indices as a function of sensor locations: (a) for the first mode, (b) for the first two modes, (c) for the first three modes, and (d) for the first four modes.

Define the actuator transfer function as $G_{ui} = \begin{bmatrix} G_{uyi} & G_{uzi} \end{bmatrix}$. Introducing (45) and the modal norms (55) to (66) one obtains the following property:

$$\|G_{ui}\|^2 \cong \alpha_{wi}^2 \sum_{k=1}^{S} \|G_{u_k yi}\|^2 \tag{67}$$

where $G_{u_k yi}$ is the transfer function of the ith mode from the kth actuator to the output y and α_{wi} is the disturbance weight of the ith mode, defined as

$$\alpha_{wi} = \sqrt{1 + \frac{\|G_{wzi}\|^2}{\|G_{wyi}\|^2}} \tag{68}$$

To show it, note that

$$\|G_{ui}\|^2 \cong \|G_{uzi}\|^2 + \|G_{uyi}\|^2 \tag{69}$$

Note also that from Eq.(45) one obtains

$$\|G_{uzi}\|^2 \cong \sum_{k=1}^{S} \|G_{u_k zi}\|^2, \quad \text{and} \quad \|G_{uyi}\|^2 \cong \sum_{k=1}^{S} \|G_{u_k yi}\|^2$$

where $G_{u_k zi}$ is the transfer function of the ith mode from the kth actuator to the performance z. Introducing the above equations to Eq.(69) we obtained the following relationship: $\|G_{ui}\|^2 \cong \sum_{k=1}^{S}\left(\|G_{u_k zi}\|^2 + \|G_{u_k yi}\|^2\right)$. Next, Eq.(66) gives

$$\|G_{u_k zi}\| \cong \frac{\|G_{u_k yi}\|\|G_{wzi}\|}{\|G_{wyi}\|}$$

which, introduced to the previous equation gives (67). Note that the disturbance weight α_{wi} does not depend on the actuator location: it characterizes structural dynamics caused by the disturbances w.

Similarly, one obtains the additive property of the sensor locations of a generalized structure. Define the sensor transfer function as $G_{yi} = \begin{bmatrix} G_{wyi} & G_{uyi} \end{bmatrix}$, thus $\|G_{yi}\|^2 \cong \|G_{wyi}\|^2 + \|G_{uyi}\|^2$, then the following property holds:

$$\|G_{yi}\|^2 \cong \alpha_{zi}^2 \sum_{k=1}^{R} \|G_{uy_k i}\|^2 \tag{70}$$

where

$$\alpha_{zi} = \sqrt{1 + \frac{\|G_{wzi}\|^2}{\|G_{uzi}\|^2}} \tag{71}$$

is the performance weight of the ith mode. Note that the performance weight α_{zi} characterizes part of the structural dynamics that is observed at the performance output; hence, it does not depend on the sensor location.

The above properties are the basis of the actuator and sensor search procedure of a generalized structure. The actuator index evaluates the actuator usefulness in test, and is defined as follows:

$$\sigma_{ki} = \frac{\alpha_{ui} \left\| G_{u_k yi} \right\|}{\left\| G_u \right\|} \tag{72}$$

where $\|G_u\|^2 = \|G_{uy}\|^2 + \|G_{uz}\|^2$, while the sensor index is

$$\sigma_{ki} = \frac{\alpha_{yi} \left\| G_{uy_k i} \right\|}{\left\| G_y \right\|} \tag{73}$$

where $\|G_y\|^2 = \|G_{uy}\|^2 + \|G_{wy}\|^2$.

The indices are the building blocks of the actuator placement matrix Σ

$$\Sigma = \begin{array}{c} \begin{bmatrix} \sigma_{11} & \sigma_{12} & \cdots & \sigma_{1k} & \cdots & \sigma_{1S} \\ \sigma_{21} & \sigma_{22} & \cdots & \sigma_{2k} & \cdots & \sigma_{2S} \\ \cdots & \cdots & \cdots & \cdots & \cdots & \cdots \\ \sigma_{i1} & \sigma_{i2} & \cdots & \sigma_{ik} & \cdots & \sigma_{iS} \\ \cdots & \cdots & \cdots & \cdots & \cdots & \cdots \\ \sigma_{n1} & \sigma_{n2} & \cdots & \sigma_{nk} & \cdots & \sigma_{nS} \end{bmatrix} \begin{array}{l} \\ \\ \\ \leftarrow i\text{th mode} \\ \\ \\ \end{array} \\ \uparrow \\ k\text{th actuator} \end{array} \tag{74}$$

and a similar matrix for sensor placement.

The placement index of the kth actuator (sensor) is determined from the kth column of Σ. In the case of the H_2 norm, it is the rms sum of the kth actuator indexes over all modes,

$$\sigma_k = \sqrt{\sum_{i=1}^{n} \sigma_{ik}^2} \tag{75}$$

$k = 1,\ldots,S$ or R, and in the case of the H_∞ and Hankel norms it is the largest index over all modes

$$\sigma_k = \max_i(\sigma_{ik}) \tag{76}$$

$i = 1, \ldots, n,\ k = 1, \ldots, S$ or R.

This property shows that the index for the set of sensors/actuators is determined from the indexes of each individual sensor or actuator. This decomposition allows for the evaluation of an individual sensor/actuator through its participation in the performance of the whole set of sensors/actuators.

Example 10. Sensor placement for a generalized structure. Consider the 3D truss as in Fig.25. The disturbance w is applied at node 7 in the horizontal direction. The

performance z is measured as rates of all nodes. The input u is applied at node 26 in the vertical direction, and the candidate sensor locations are at the nodes 5, 6, 7, 12, 13, 14, 19, 20, 21, 26, 27, and 28 in all three directions (total of 36 locations). Using the first 50 modes, the task is to select a low number of sensors that would measure, as close as possible, the disturbance-to-performance dynamics.

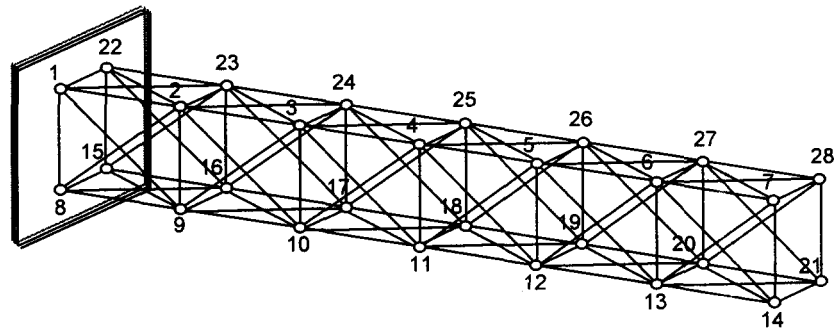

Figure 25. A 3D truss structure.

First, the H_∞ norms of each mode of G_{wz}, G_{wy}, G_{uz}, and G_{uy} are determined and presented in Fig.26a,b. Next, the validity of Eq.(66) is checked. Indeed, it holds since the plots of $g_1(k) = \|G_{wzk}\|_\infty \|G_{uyk}\|_\infty$ and of $g_2(k) = \|G_{wyk}\|_\infty \|G_{uzk}\|_\infty$ overlap in Fig.27.

Next, the sensor weights α_{yi} are determined for each mode, and shown in Fig.28. The placement indices σ_k for each sensor are determined from (76), and their plot is shown in Fig.29. Note that some sensors with a high value of σ_k are highly correlated. After removing the highly correlated locations, the two locations $k = 29$ and $k = 30$ remained. They correspond to node 14 in the y- and z-directions.

7.6. SIMULTANEOUS PLACEMENT OF ACTUATORS AND SENSORS

Simultaneous selection of sensor and actuator locations is an issue of certain importance, since fixing the locations of sensors while placing actuators (or vice versa) limits the improvement of system performance. The presented placement algorithm is developed for structures using either H_2, H_∞, or Hankel modal norms. The algorithm consists of determination of either H_2, H_∞, or Hankel norms for a single mode, single actuator, and single sensor. Based on these norms the sensor and actuator placement matrices are generated for each considered mode to evaluate sensor and actuator combinations, and to determine the simultaneous actuator and sensor locations that maximize each modal norm.

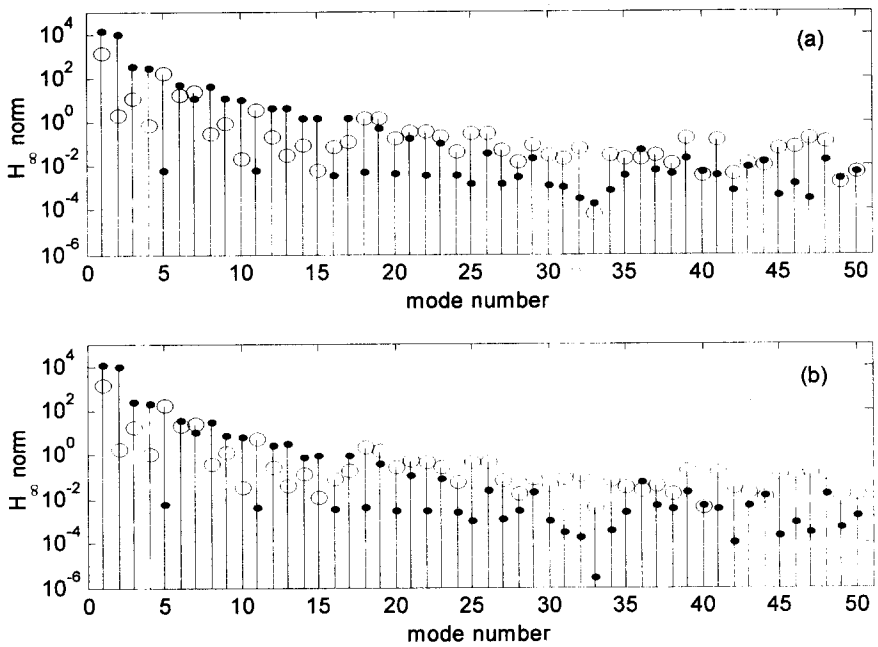

Figure 26. The H_∞ norms of the 3D truss modes: (a) G_{wz} (•) and G_{uy} (○); and (b) G_{wy} (•) and G_{uz} (○)

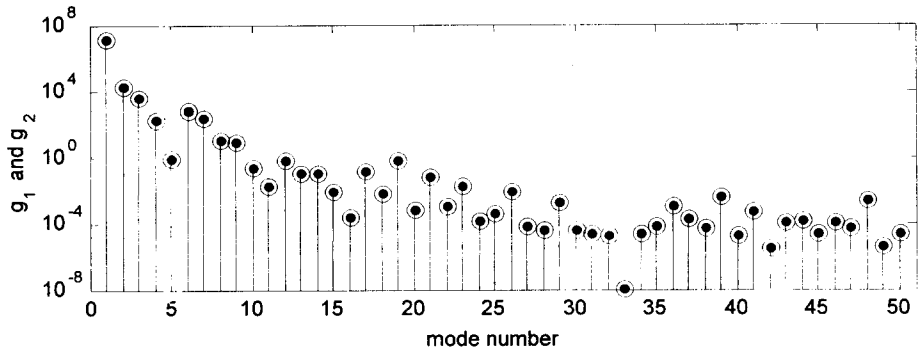

Figure 27. Overlapped plots of $g_1(k)$ (•) and $g_2(k)$ (○) show that Eq.(66) holds.

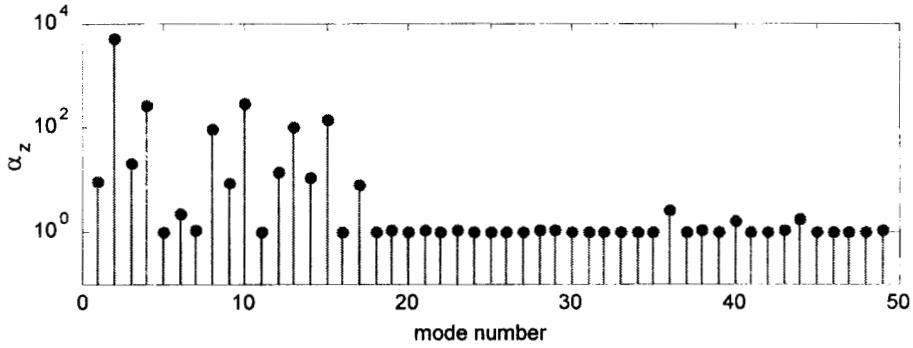

Figure 28. Modal weights for the 3D truss to accommodate disturbances in the generalized model.

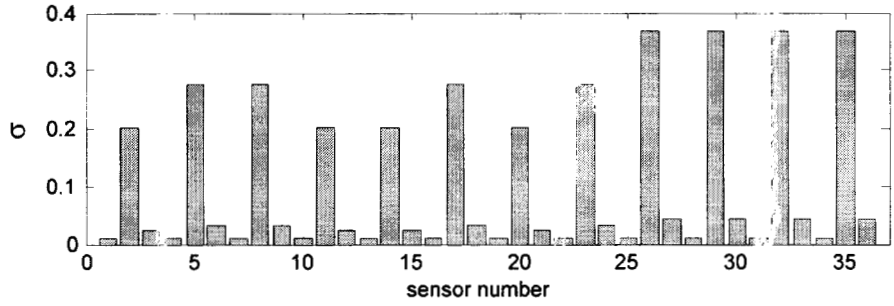

Figure 29. Sensor indices for the 3D truss show the importance of each sensor.

In this section the symbol $\|.\|$ will denote either H_2, H_∞, or Hankel norm. For the set R of the candidate actuator locations, one shall select a subset r of actuators, and concurrently for the set S of the candidate sensor locations, one shall select a subset s of sensors. The criterion is the maximization of the system norm.

Recall that the norm $\|G_{ijk}\|$ characterizes the ith mode equipped with the jth actuator and the kth sensor. Previously we defined the placement index for actuators and for sensors separately, see Eqs.(56) and (58). Here, for each mode, we define the actuator and sensor placement index

$$\sigma_{ijk} = \frac{\|G_{ijk}\|}{\|G_{mi}\|}, \qquad i = 1, \ldots, n \tag{77}$$

The placement index σ_{ijk} is a measure of the participation of the jth actuator and the kth sensor in the impulse response of the ith mode. Using this index the actuator and sensor placement matrix of the ith mode is generated

$$\Sigma_i = \begin{array}{c} \begin{bmatrix} \sigma_{i11} & \sigma_{i12} & \cdots & \sigma_{i1k} & \cdots & \sigma_{i1S} \\ \sigma_{i21} & \sigma_{i22} & \cdots & \sigma_{i2k} & \cdots & \sigma_{i2S} \\ \cdots & \cdots & \cdots & \cdots & \cdots & \cdots \\ \sigma_{ij1} & \sigma_{ij2} & \cdots & \sigma_{ijk} & \cdots & \sigma_{ijS} \\ \cdots & \cdots & \cdots & \cdots & \cdots & \cdots \\ \sigma_{iR1} & \sigma_{iR2} & \cdots & \sigma_{iRk} & \cdots & \sigma_{iRS} \end{bmatrix} \begin{array}{l} \\ \\ \\ \leftarrow j\text{th actuator} \\ \\ \\ \end{array} \\ \uparrow \\ k\text{th sensor} \end{array} \tag{78}$$

$i=1,\ldots,n$. For the ith mode the jth actuator index σ_{aij} is the rms sum over all selected sensors, and the kth sensor index σ_{sik} is the rms sum over all selected actuators

$$\sigma_{aij} = \sqrt{\sum_{k=1}^{s} \sigma_{ijk}^2}, \qquad \sigma_{sik} = \sqrt{\sum_{j=1}^{r} \sigma_{ijk}^2} \tag{79}$$

These indices, however, cannot be readily evaluated since for evaluation of the actuator index one needs to know the sensor locations (which have not been yet selected), and vice versa. This difficulty can be overcome by using the property similar to Eq.(66). Namely, for the placement indices we obtain

$$\sigma_{ijk}\sigma_{ilm} \cong \sigma_{ijm}\sigma_{ilk} \tag{80}$$

This property can be proven by the substitution of the norms as either in Eq.(38), (39) or (40) into the above equation.

It follows from this property that by choosing the two largest indices for the ith mode, say σ_{ijk} and σ_{ilm} (such that $\sigma_{ijk} > \sigma_{ilm}$), the corresponding indices σ_{ijm} and σ_{ilk} are also large. In order to show it, note that $\sigma_{ilm} \le \sigma_{ijm} \le \sigma_{ijk}$ holds and $\sigma_{ilm} \le \sigma_{ilk} \le \sigma_{ijk}$ also holds as a result of (80) and the fact that $\sigma_{ijm} \le \sigma_{ijk}$ and $\sigma_{ilk} \le \sigma_{ijk}$. In consequence, by selecting individual actuator and sensor locations with the largest indices one automatically maximize the indices (79) of the sets of actuators and sensors.

The determination of locations of large indices is illustrated with the following example. Let σ_{124}, σ_{158}, and σ_{163} be the largest indices selected for the first mode. They correspond to 2, 5, and 6 actuator locations and 3, 4, and 8 sensor locations. They are marked in dark color in Fig.30. According to (80) the indices σ_{123}, σ_{128}, σ_{153}, σ_{154}, σ_{164}, and σ_{168} are also large. They are marked in white color with white spots in Fig.30. Now we see that the rms summation for actuators is over all selected sensors (3, 4, and 8), the rms summation for sensors is for over all selected actuators (2, 5, and 6), and that both summations maximize the actuator and sensor indices.

Example 11. Simultaneous placement of actuator and sensor for a clamped beam as in Fig.21. The candidate actuator locations are the vertical forces at nodes 1 to 14 and the candidate sensor locations are the vertical rate sensors located at nodes 1 to 14. Using the

H_∞ norm and considering the first four modes, we shall determine at most 4 actuator and 4 sensor locations (one for each mode).

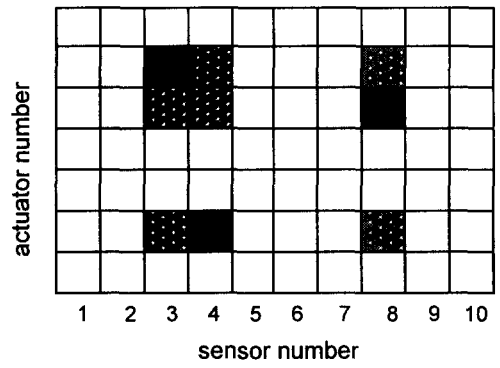

Figure 30. An example of the actuator and sensor placement matrix for the first mode; the largest indices are dark, and the large indices are dark with white spots.

In this example n=4 and R=S=14. Using Eqs.(79) the placement matrices for the first four modes were determined and plotted in Figs.31a-d. Before the placement procedure is applied the accuracy of Eq.(80) is checked. For this purpose the second mode is chosen, i.e., i=2, and the following actuator and sensor locations are selected: j=k=3, l=m=q, and q=1,...,14. For these parameters Eq.(80) is as follows

$$\sigma_{233}\sigma_{2qq} \cong \sigma_{23q}\sigma_{2q3}$$

q=1,...,14. The plots of the left- and right-hand side of the above equations are shown in Fig.32, showing good coincidence.

The maximal values of the actuator and sensor index in the placement matrix determine the preferred location of the actuator and sensor for each mode. Note that for each mode four locations – two sensor locations and two actuator locations – have the same maximal value. Moreover, they are symmetrical with respect to the beam center, see Fig.31. We selected four collocated sensors and actuators at the left-hand side of the beam center, one for each mode. Namely, for mode 1 – node 8, for mode 2 – node 4, for mode 3 – node 3, and for mode 4 – node 2.

7. Modal Actuators and Sensors

In some structural tests it is desirable to isolate (i.e., excite and measure) a single mode. Such technique considerably simplifies the determination of modal parameters, see Ref.[13]. This was first achieved by using the force appropriation method, called also the Asher method, see [11], or phase separation method, see [3]. In this method a spatial distribution and the amplitudes of a harmonic input force are chosen to excite a single structural mode. Modal actuators or sensors were presented also in [4], [10], and [8] with application to structural acoustic problems. This section follows Ref.[6].

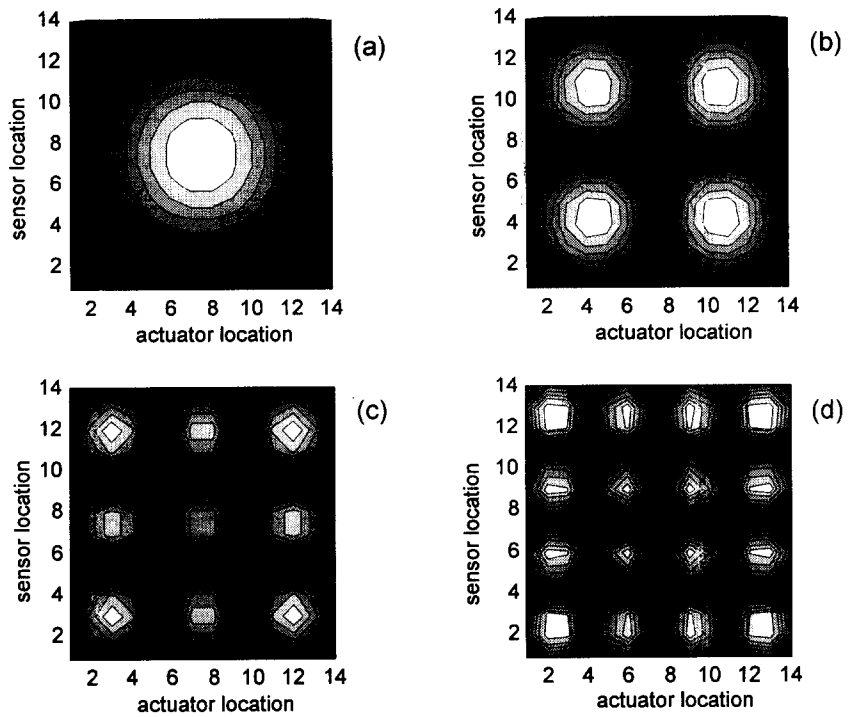

Figure 31. Actuator and sensor placement matrix, with dark color representing the high value of its entries, and locations of the largest (actuator, sensor) placement indices being: (a) (8,8), (7,7), (7,8), and (8,7) for mode 1, (b) (4,4), (4,11), (11,11), (11,4) for mode 2, (c) (12,12), (3,12), (12,3), (3,3) for mode 3, and (d) (2,2), (2,13), (13,2), (13,13) for mode 4

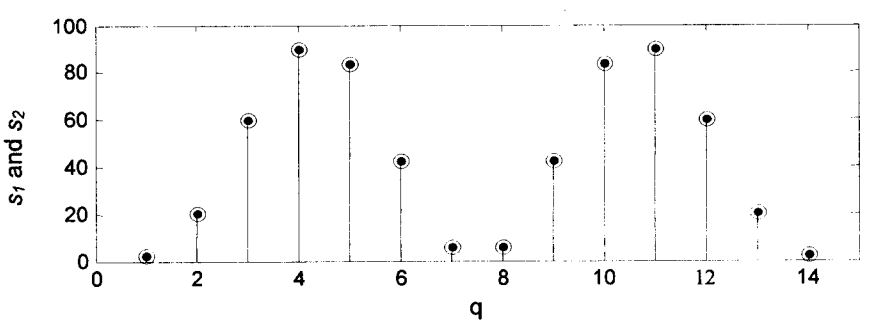

Figure 32. The verification of Eq.(80): O denotes $s_1 = \sigma_{233}\sigma_{2qq}$, • denotes $s_2 = \sigma_{23q}\sigma_{2q3}$, and $s_1 = s_2$.

In this section we present a technique to determine the actuator or sensor locations and their gains to excite and sense a target mode or a set of targeted modes. The technique is based on the relationship between the modal and nodal coordinates of the actuator or sensor locations. Being distinct from the force appropriation method it does not require the input force to be a harmonic one. Rather, it determines the actuator locations and actuator gains, while the input force time history is irrelevant (modal actuator or sensor acts as a filter). The locations and gains, for example, can be implemented as a width-shaped piezoelectric film. Finally, the method allows for excitation and observation of not only a single structural mode but also of a set of selected modes, each one with the assigned amplitude.

A structural model in this section is described by the second order modal model, see Eq.(7). In modal coordinates the equations of motion of each mode are decoupled, as in Eq.(10). Thus if the modal input gain is zero, the mode is not excited; if the modal output gain is zero, the mode is not observed. This simple physical principle is the base for the more specific description of the problem in the following sections.

7.1. MODAL ACTUATORS

The task in this section is to determine the locations and gains of the actuators such that n_m modes of the system are excited with approximately the same amplitude, where $1 \le n_m \le n$, and n is the total number of considered modes. This task is solved using the modal equations (7) or (10). Note that if the ith row, b_{mi}, of the modal input matrix, B_m, is zero the ith mode is not excited. Thus, by assigning the entries of b_{mi} either 1 or 0 one makes the ith mode either excited or not. For example, if one wants to excite the first mode only, B_m is a one-column matrix of a form $B_m = [1 \quad 0 \quad \cdots \quad 0]^T$. On the other hand, if one wants to excite all modes independently and equally, one assigns a unit matrix, $B_m = I$.

Given (or assigned) the modal matrix B_m, the nodal matrix B_o is derived from Eq.(8) . Equation (8) can be re-written as follows

$$B_m = RB_o \tag{81}$$

where $R = M_m^{-1}\Phi^T$ and matrix R is of dimensions $n \times n_d$. Recall that the number of assigned modes is $n_m \le n$. If the assigned modes are controllable, i.e. the rank of R is n_m, the least-square solution of Eq.(81) is

$$B_o = R^+ B_m \tag{82}$$

In the above equation R^+ denotes the pseudoinverse of R, i.e., $R^+ = V\Sigma^{-1}U^T$ where U, Σ, and V are obtained from the singular value decomposition of R, i.e., $R = U\Sigma V^T$.

The input matrix B_o in Eq.(82) defines the modal actuator and it can be determined alternatively from the following equation

$$B_o = M\Phi B_m \tag{83}$$

which does not require pseudoinverse and is equivalent to Eq.(81). Indeed, left-multiplication of Eq.(83) by Φ^T gives $\Phi^T B_o = \Phi^T M \Phi B_m$ or $\Phi^T B_o = M_m B_m$. Left-multiplication of the latter equation by M_m^{-1} results in Eq.(81).

Example 12. Modal actuator for a beam, single mode case. Consider a clamped beam as in Fig.21. The vertical displacement sensors are located at nodes from 2 to 15 and the single output is a sum of the sensor readings. Actuator locations shall be determined such that the second mode with modal gain of 0.01 is excited while the remaining modes are not excited. The first nine modes are considered.

The assigned modal matrix is in this case $B_m^T = [0 \quad 0.01 \quad 0 \quad 0 \quad 0 \quad 0 \quad 0 \quad 0 \quad 0]^T$. From (82), for this modal input matrix, a nodal input matrix B_o is determined. It contains gains for the vertical forces at the nodes from 2 to 15. The gain distribution of the actuators is shown in Fig.33a. Note that this distribution is proportional to the displacements of the second mode shape. This distribution can be implemented as an actuator with a gain proportional to its width. Thus the shape of an actuator that excites the second mode is shown in Fig.33b.

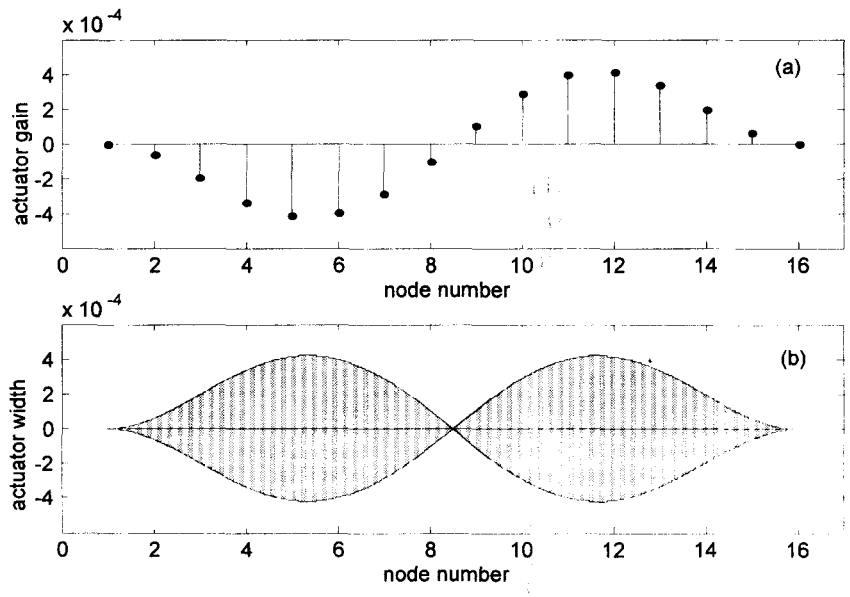

Figure 33. Actuator gains (a) and the corresponding actuator width (b) that excite the second mode.

For the above input and output the magnitude of the transfer function are presented in Fig.34. The plot shows clearly that only the second mode is excited.

If one wants to excite the ith mode with certain amplitude, say a_i, the H_∞ norm can be used as a measure of the amplitude of the ith mode. In case of a single-input-single-

output system, the H_∞ norm of the ith mode is equal to the height of the ith resonance peak. In case of multiple inputs (or outputs) the H_∞ norm of the ith mode is approximately equal to the root-mean-square sum of the ith resonance peaks corresponding to each input (or output). It is approximately determined as follows

$$\|G_i\|_\infty \cong \frac{\|B_{mi}\|_2 \|C_{mi}\|_2}{2\zeta_i\omega_i} = \frac{\|b_{mi}\|_2 \|c_{mi}\|_2}{2\zeta_i\omega_i} \tag{84}$$

see (39).

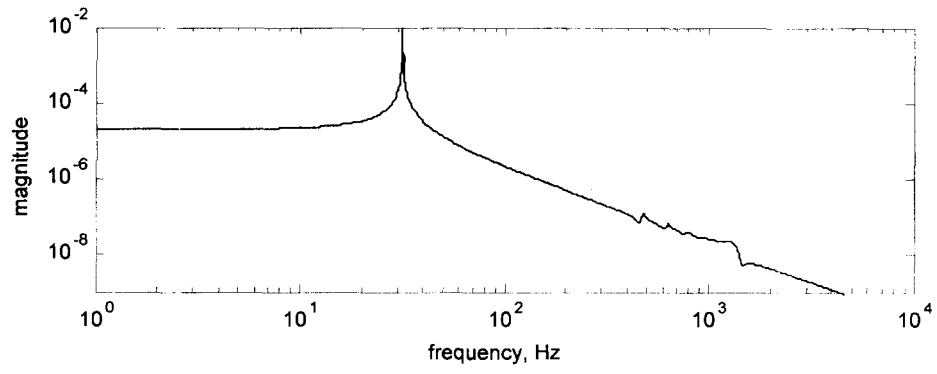

Figure 34. Magnitude of a transfer function with the second-mode modal actuator: only the second mode is excited.

Assume a unity input gain for the current mode, i.e. $\|b_{mi}\|_2 = 1$, so that the current amplitude a_{oi} is

$$a_{oi} = \frac{\|c_{mi}\|_2}{2\zeta_i\omega_i} \tag{85}$$

In order to obtain amplitude a_i one has to multiply a_{oi} by the weight w_i, such that $a_i = w_i a_{oi}$. Introducing (85) to the latter equation one obtains the weight

$$w_i = \frac{2a_i\zeta_i\omega_i}{\|c_{mi}\|_2} \tag{86}$$

Define the weight matrix $W = diag(w_1, w_2, \ldots, w_n)$, then the matrix that sets the required output modal amplitudes is

$$B_{mw} = WB_m \tag{87}$$

Example 13. Modal actuator for a beam, multiple mode case. All nine modes of the same beam need to be excited with the amplitude of 0.01 by a single actuator. For this case, the matrix B_m is as follows $B_m^T = 0.01 \times [1 \;\; 1 \;\; 1 \;\; 1 \;\; 1 \;\; 1 \;\; 1 \;\; 1 \;\; 1]^T$ and the weighting matrix is obtained from Eq.(86). The resulting gains of the nodal input matrix B_o (shown in Fig.35a) do not follow any particular mode shape. The width of an actuator that corresponds to the input matrix B_o and excites all nine modes is shown in Fig.35b.

The plot of the transfer function of the single-input system with the input matrix B_o is shown in Fig.36. The plot shows that all nine modes are indeed excited, with approximately the same amplitude of 0.01 cm.

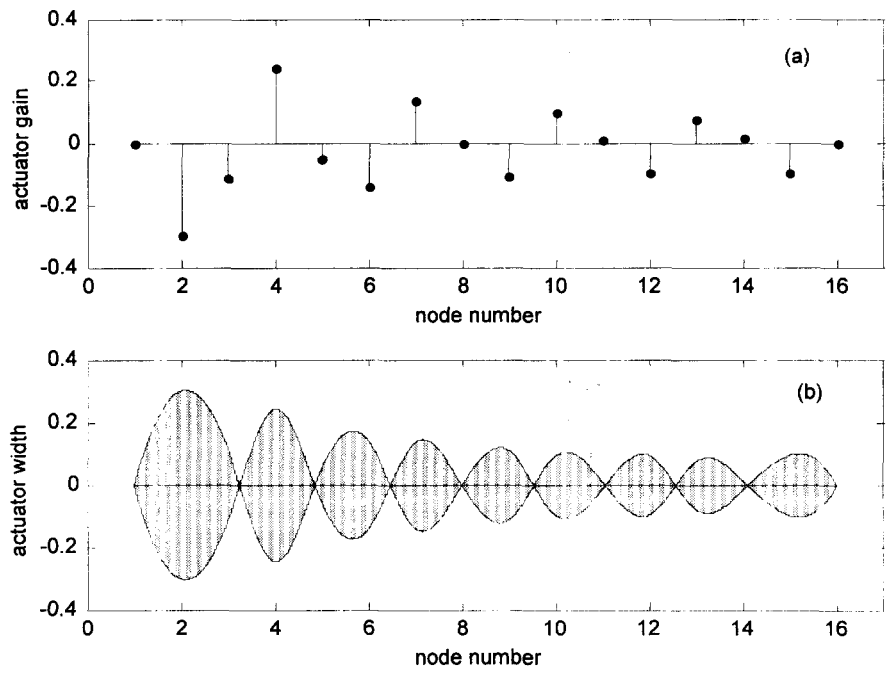

Figure 35. Actuator gains (a), and corresponding actuator width that excites all nine modes.

7.2. MODAL SENSORS

The modal sensor determination is similar to the determination of modal actuators. The governing equations are derived from Eq.(9)

$$C_{mq} = C_{oq}\Phi, \quad C_{mv} = C_{ov}\Phi \tag{88}$$

If one wants to observe a single mode only (say ith mode), one assumes the modal output matrix is in the form $C_{mq} = [0 \;\; \ldots \;\; 0 \;\; 1 \;\; 0 \;\; \ldots \;\; 0]$, where 1 stands at the ith

position. If one wants to observe n_m modes one assumes the modal output matrix is in the form $C_{mq} = \left[c_{q1}, c_{q2}, \ldots, c_{qn}\right]$, where $c_{qi} = 1$ for selected modes, otherwise $c_{qi} = 0$. The corresponding output matrix is obtained from (88)

$$C_{oq} = C_{mq}\Phi^{+} \tag{89}$$

where Φ^{+} is the pseudoinverse of Φ. Similarly, one obtains the rate sensor matrix C_{ov} for the assigned modal rate sensor matrix C_{mv}

$$C_{ov} = C_{mv}\Phi^{+} \tag{90}$$

Above we assumed that the assigned modes are observable, i.e. that the rank of Φ is n_m, where n_m is the number of the assigned modes.

The following are alternative equations for determination of modal sensors

$$C_{oq} = C_{mq}M_m^{-1}\Phi^T M, \quad C_{ov} = C_{mv}M_m^{-1}\Phi^T M \tag{91}$$

These equations are equivalent to Eqs.(88). Indeed, right-multiplication of the first equation of (91) by Φ gives $C_{oq}\Phi = C_{mq}M_m^{-1}\Phi^T M\Phi$, hence $C_{oq}\Phi = C_{mq}M_m^{-1}M_m$, consequently $C_{oq}\Phi = C_{mq}$, i.e., the first equation of (88) is obtained. Similarly one can show the equivalence of the second equation of (91) and (88).

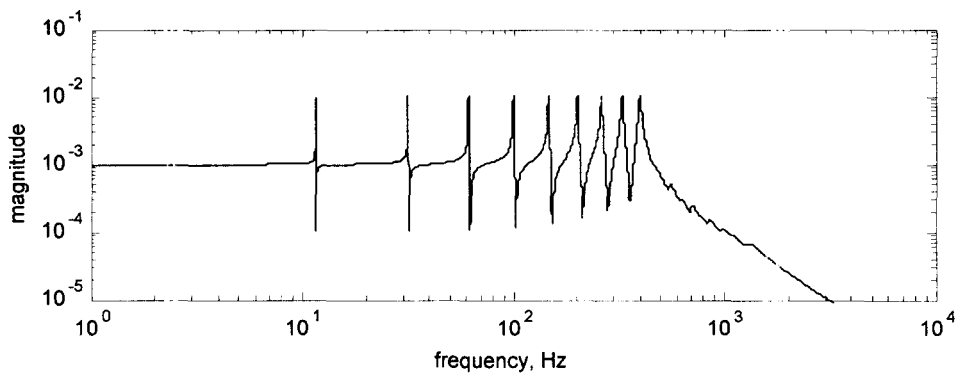

Figure 36. Magnitude of a transfer function for the nine-mode modal actuator shows the nine resonances of the excited modes.

Multiple modes with assigned modal amplitudes a_i are obtained using the sensor weights. The weighted sensors are obtained from equation similar to Eq.(86). Namely, the ith weight is determined from the following equation

$$\|c_{mi}\|_2 = \frac{2\zeta_i \omega_i a_i}{\|b_{mi}\|_2} \tag{92}$$

where a_i is the amplitude of the ith mode.

Example 14. Modal sensors for a beam and for all modes. The beam from Fig.21 with three vertical force actuators located at nodes 2, 7, and 12 is considered. The task is to find the displacement output matrix C_{oq} such that the first nine modes have equal contribution to the measured output with amplitude 0.01.

The matrix C_{mq} that excites the first nine modes is the unit matrix of dimension 9 of amplitude a_i=0.01, i.e., $C_{mq} = 0.01 \times W \times I_9$. The gains that make the mode amplitudes approximately equal are determined from Eq.(92). The output matrix C_{oq} is determined from Eq.(89). For this matrix the magnitudes of the transfer functions of the 9 outputs in Fig.37 show that all nine of them have a resonance peak of 0.01.

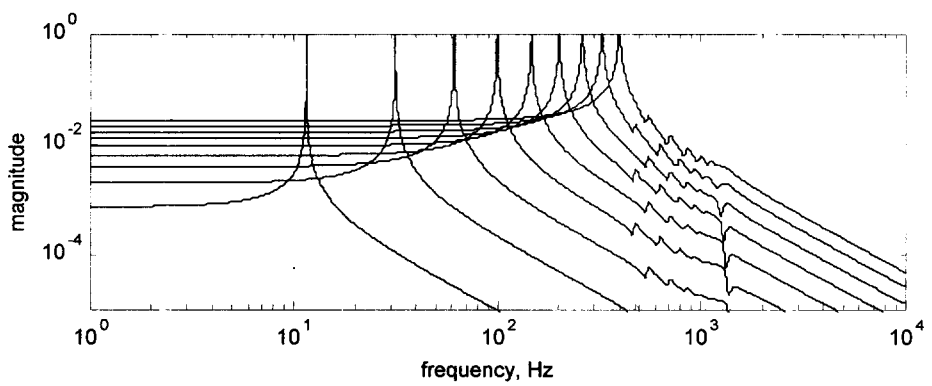

Figure 37. Magnitude of the transfer function with the nine single-mode sensors.

Example 15. Modal sensors for a beam, for all but one mode. The beam with actuators as in Example 14 is considered. Find the nodal rate sensor matrix C_{ov} such that all nine modes but mode 2 contribute equally to the measured output with the amplitude of 0.01.

The matrix C_{mv} that gives in the equal resonant amplitudes of 0.01 is as follows: $C_{mv} = 0.01 \times W \times [1 \quad 0 \quad 1 \quad 1 \quad 1 \quad 1 \quad 1 \quad 1 \quad 1]$, where the weight W is determined from (92) and the output matrix C_{ov} is obtained from (90). For this matrix the magnitude of the transfer function is shown in Fig.38, dashed line. This magnitude is compared with the magnitude of the transfer function for the output that contains all the 9 modes (solid line). It is easy to notice that the second resonance peak is missing in the plot.

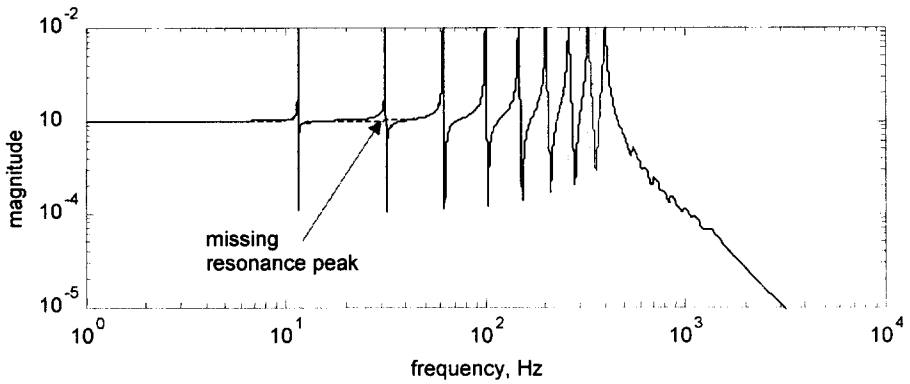

Figure 38. Magnitude of the transfer function with the nine-mode sensor (solid line), and with the eight-mode sensor where the second mode is missing (dashed line).

8. Conclusions

In this paper we discussed the importance of locations and gains of sensors and actuators in structural dynamics. They impact the controllability and observability of a structure and its norms. Using modal state space representation the norms can be used to locate sensors and actuators for structural testing and control, and to sense and/or excite a single mode or a set of selected modes.

Acknowledgements

The research described in this paper was carried out at the Jet Propulsion Laboratory, California Institute of Technology, under a contract with the National Aeronautics and Space Administration.

References

1. Boyd, S.P., and Barratt, C.H. (1991) *Linear Controller Design*, Prentice Hall, Englewood Cliffs, NJ.
2. Clough, R. W., and Penzien, J. (1975) *Dynamics of Structures*, McGraw-Hill, New York.
3. Cooper, J.E. and Wright, J.R. (1997) To fit or to tune? That is the question, *Proc. 15th International Modal Analysis Conf.*, Orlando, FL, pp.1353-1359.
4. Friswell, M.I. (2001) On the design of modal actuators and sensors, *Journal of Sound and Vibration,* vol.241, No.3, pp.361-372.
5. Gawronski, W. (1998) *Dynamics and Control of Structures. A Modal Approach.* Springer, New York.
6. Gawronski, W. (2000) Modal actuators and sensors, *Journal of Sound and Vibration*, vol. 229, no.4, pp.1013-1022.
7. Hatch, M.R. (2000) *Vibration Simulation Using Matlab and ANSYS,* Chapman and Hall/CRC, Boca Raton.

8. Hsu, C.-Y., Lin, C.-C. and Gaul, L., (1998) Vibration and sound radiation controls of beams using layered modal sensors and actuators, *Smart Materials and Structures*, vol.7, pp.446-455.
9. Kailath, T. (1980) *Linear Systems*, Prentice Hall, Englewood Cliffs, NJ.
10. Lee, C.-K. and Moon, F.C. (1990) Modal sensors/actuators, *J. of Applied Mechanics, Trans. ASME*, vol. 57, pp.434-441.
11. Maia, N.M.M., and Silva, J.M.M. (Eds.), (1997) *Theoretical and Experimental Modal Analysis*, Research Studies Press Ltd., Taunton, England.
12. Moore, B.C. (1981) Principal component analysis in linear systems, controllability, observability and model reduction, *IEEE Trans. Autom. Control*, vol.26, pp.17-32.
13. Phillips, A.W., and Allemang, R.J. (1996) Single degree-of-freedom modal parameter estimation methods. *Proc. 14th International Modal Analysis Conf.*, Deaborn, MI, pp.253-260.
14. Preumont, A. (1997) *Vibration Control of Active Structures*, Kluwer Academic Publishers, Dordrecht.
15. Skogestad, S., and Postlethwaite, I. (1996) *Multivariable Feedback Control,* Wiley, Chichester, England.
16. Van de Wal, M., and de Jager, B. (2001) A review of methods for input/output selection, *Automatica,* vol.37, pp.487-510.
17. Zhou, K., and Doyle, J.C. (1998) *Essentials of Robust Control,* Prentice Hall, Upper Saddle River, NJ.